Journal of Structural Biology: X 5 (2021) 100051

Contents lists available at ScienceDirect

Journal of Structural Biology: X

journal homepage: www.sciencedirect.com/journal/journal-of-structural-biology-x

The dorsal tergite cuticle of *Helleria brevicornis:* Ultrastructure, mineral distribution, calcite microstructure and texture

Bastian Seidl [a], Christian Reisecker [b], Frank Neues [c], Alessandro Campanaro [d], Matthias Epple [c], Sabine Hild [b], Andreas Ziegler [a,*]

[a] Central Facility for Electron Microscopy, University of Ulm, Albert-Einstein-Allee 11, 89069 Ulm, Germany
[b] Department of Polymer Science, Johannes Kepler University Linz, Altenbergerstraße 69, 4040 Linz, Austria
[c] Institute of Inorganic Chemistry and Center for Nanointegration Duisburg-Essen (CeNIDE), University of Duisburg-Essen, Universitätsstrasse 5-7, 45117Essen, Germany
[d] Council for Agricultural Research and Economics, Research Centre for Plant and Certification, Via di Lanciola 12/a, I-50125 Cascine del Riccio, Florence, Italy

ARTICLE INFO

Keywords:
Biomineralisation
Biological material
Calcite
Crustacea
Cuticle
Exoskeleton
Isopoda
Ultrastructure

ABSTRACT

Among the terrestrial Crustacea, isopods have most successfully established themselves in a large variety of terrestrial habitats. As in most Crustacea, their cuticle consists of a hierarchically organised organic phase of chitin-protein fibrils, containing calcium carbonate and some calcium phosphate. In previous studies, we examined the tergite cuticle of *Tylos europaeus,* which lives on seashores and burrows into moist sand. In this study, we investigate the closely related species *Helleria brevicornis,* which is completely terrestrial and lives in leaf litter and humus and burrows into the soil. To get deeper insights in relation between the structure of the organic and mineral phase in species living in diverse habitats, we have investigated the structure, and the chemical and crystallographic properties of the tergite cuticle using various preparation techniques, and microscopic and analytical methods. The results reveal long and short epicuticular sensilla with brushed tips on the tergite surface that do not occur in *T. europaeus.* As in *T. europaeus* a distal exocuticle, which contains a low number of organic fibres, contains calcite while the subjacent layers of the exo- and endocuticle contain amorphous calcium carbonate. The distal exocuticle contains a polygonal pattern of mineral initiation sites that correspond to interprismatic septa described for decapod crabs. The shape and position of calcite units do not follow the polygonal pattern of the septa. The results indicate that the calcite units form by crystallisation from an amorphous phase that progresses from both margins of the septa to the centres of the polygons.

1. Introduction

Crustaceans have an exoskeleton, the cuticle, which in most species consists of an organic matrix reinforced by mineral phases. Because of its excellent mechanical properties, hierarchical organisation and functional versatility crustacean cuticle has gained high interest for biomimetic approaches for the development of composites with improved and adjusted functional properties (Fabritius et al., 2016; Grunenfelder et al., 2014; Nikolov et al., 2010; Nikolov et al., 2011).

The organic matrix of the crustacean cuticle is organized in at least 7 hierarchical levels (Nikolov 2011). It consists of N-acetyl-glucosamine molecules that form anti-parallel chains of crystalline α-chitin nanofibrils. These fibrils are surrounded by a thin layer of protein (Blackwell and Weih, 1980; Carlström, 1957; Neville et al., 1976). Depending on the species, several chitin-protein fibrils can form larger fibres. The fibrils or fibres are arranged parallel to each other forming planes oriented horizontally to the cuticle surface (Fabritius et al., 2016). In general, these planes pile up helically at an angle and form a twisted plywood structure (Bouligand, 1972). In sections through the cuticle, the twisted plywood structure leads to a virtual lamella pattern in which the thickness of these lamellae results from the distance in which the angles of fibre rotation cover 180°. This distance is called stacking height. These helicoidally stacked fibrils or fibres form an outer exocuticle, an underlying endocuticle and sometimes an innermost membranous layer. The outermost layer of the cuticle, the epicuticle, consist of proteins and hydrocarbons, has no such stacks and contains no chitin. It forms epicuticular scales and sensory setae (Holdich and Lincoln, 1974; Price and Holdich, 1980). The exo- and endocuticle are mineralized with magnesian calcite, amorphous calcium carbonate and minor amounts of calcium phosphate (Becker et al., 2005; Neues et al., 2007).

* Corresponding author at: Central Facility for Electron Microscopy, University of Ulm, Albert-Einstein-Allee 11, 89069 Ulm, Germany.
E-mail address: andreas.ziegler@uni-ulm.de (A. Ziegler).

https://doi.org/10.1016/j.yjsbx.2021.100051
Received 5 July 2021; Accepted 6 July 2021
Available online 10 July 2021

As in all arthropods, the crustacean cuticle forms skeletal elements such as antennae, legs, jaws, claws and much more, with different functions. The shape, structure and composition of the cuticle in these skeletal elements depend on the phylogenetic position of the species and are evolutionary adapted to function, and the behaviour and habitat of the animal. Isopods inhabit a large variety of different habitats, including various seawater, freshwater and terrestrial habitats (Edney, 1968). In fact, terrestrial isopods or Oniscidea are the only crustaceans living completely independent of limbic, marine or river water. Oniscidea live in almost all terrestrial habitats from beaches, mesic habitats of woodlands, high altitudes and even deserts (Edney, 1968). One important aspect defining the requirements towards the isopod cuticle is

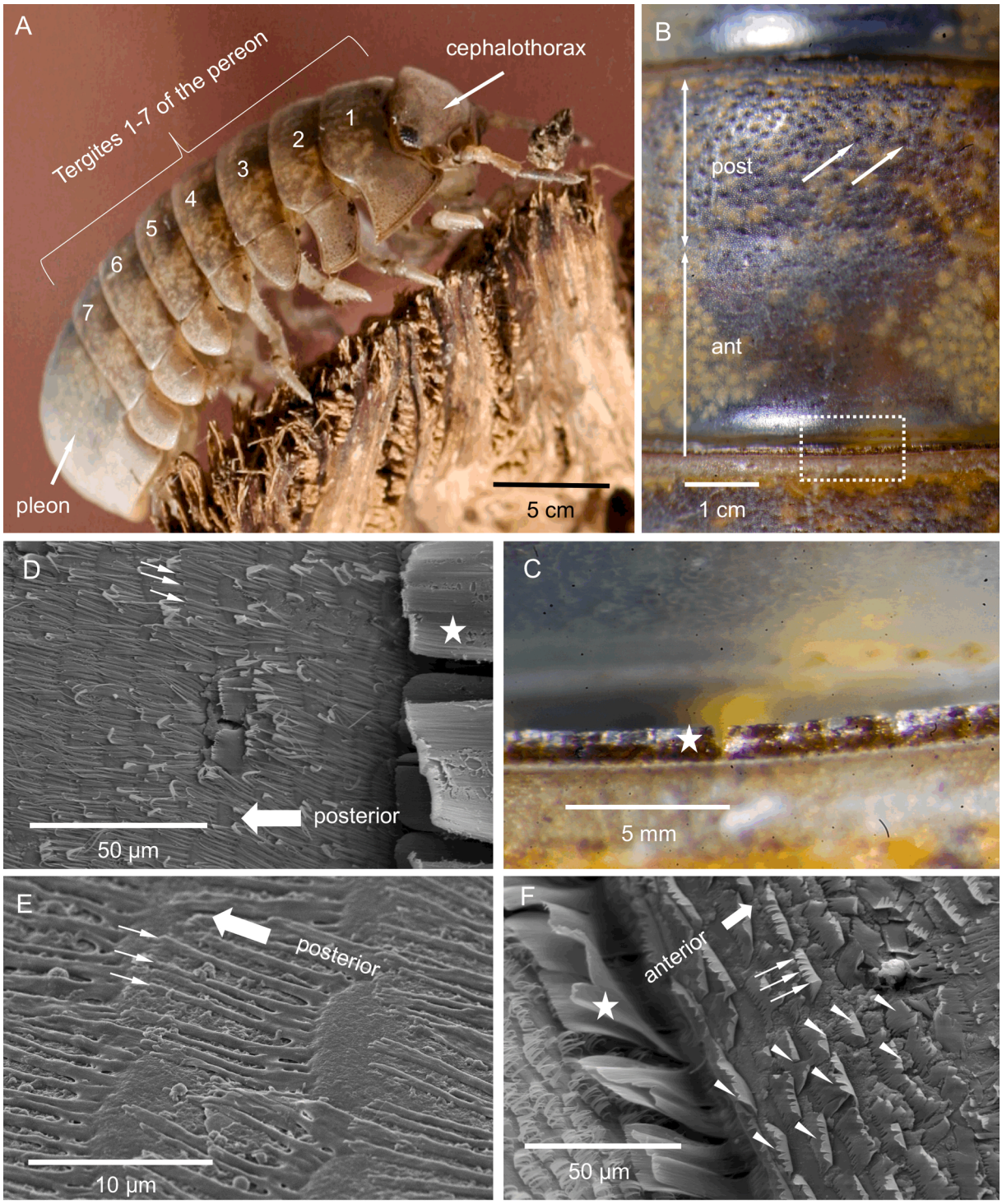

Fig. 1. The structure of tergites and their epicuticular scales; A-C: light micrographs and D-F: SEM micrographs. A) *Helleria brevicornis* depicting the cephalothorax, the pereon tergites 1–7 and the pleon. B) The tergites are divided in smooth anterior part (ant) and posterior part (post) carrying numerous sensilla (large arrows) visible as small dark spots. C) A detail of the region marked with a dashed rectangle in B depicting a row of large scales at the posterior side of the tergite (white asterisk in C, D and F). D, E) The surface of the tergite is covered with pectinate scales, with the comb teeth oriented to the posterior side (small arrows). F) Several rows of scales (arrowheads) at the posterior margin of the tergite point to the opposite, i.e. the anterior direction. The comb teeth (small arrows) are partly fused; bending at the tips is likely a drying artefact.

the behaviour to prevent predation. Some terrestrial isopods have long legs and can run away upon predation while others have a flat body and cling themselves to the substrate to make it hard for predators to grasp the prey and to reach the more vulnerable ventral side (Schmalfuss, 1984). Others have short legs and walk slowly, but can roll up into a perfect ball to hide the antenna, legs and ventral side, making it difficult for a predator to grab the animal and puncture the cuticle (Schmalfuss, 1984).

Helleria brevicornis is a remarkable species. It belongs to the monophyletic family Tylidae (Dimitriou et al., 2019; Erhard, 1997). *H. brevicornis* is the only known species of the genus *Helleria*. All other Tylidae are representatives of the genus *Tylos*. Most of the latter live on sandy beaches were they burrow into the moist sand, but some of them live in rocky crevices exposed to tidal spray (Schmalfuss and Ferrara, 1978). In contrast, *H. brevicornis* lives in forests within leaf litter and humus and burrows into the soil. It is found at elevations from sea level to 1200 m (Vandel, 1960). Its original geographic distribution is restricted to Sardinia and Corsica, while very recent colonization of spotted continental locations in France and Italy and of some islands of the Tuscan archipelago are possibly driven by human transport (Gentile et al., 2010). Molecular features and many morphological characteristics that separate *H. brevicornis* from all other terrestrial isopods suggest an ancient divergence from the lineage to other terrestrial isopods (Collinge, 1941; Michel-Salzat and Bouchon, 2000; Vandel, 1960). All Tylidae including *H. brevicornis* can roll into a perfect sphere. (Schmalfuss, 1984; Schmalfuss and Ferrara, 1978), so that a predator can only reach the dorsal cuticle of the cephalothorax, the pereon and the pleon (Fig. 1A). The tergites form the dorsal sclerites of the pereon and pleon of isopods (Fig. 1A). In rolling species, the tergites are particularly thick and mechanically strong, and have a higher ratio of mineral to organic material than species that cannot role into a sphere (Becker et al., 2005; Hild et al., 2008; Seidl et al., 2011).

In previous studies we have analysed the tergite cuticle of *Tylos europaeus* (Seidl et al., 2011; Seidl et al., 2012; Seidl et al., 2018) which composition, ultrastructure and crystallographic properties of calcite is distinct from other evolutionary more derived taxa of terrestrial isopods (Hild et al., 2008; Hild et al., 2009; Seidl and Ziegler, 2012; Seidl et al., 2012). In the present study, we describe such properties of the tergite cuticle of *H. brevicornis*. In particular, we are interested in 1) whether these features are common to both genera of the Tylidae, 2) whether there are differences due to the different habitats of the two species, and 3) the relation between organic structures and calcite-crystal shape and distribution. For the analysis, we used a variety of different preparation methods and analysed the cuticle by transmission (TEM), scanning transmission (STEM) and scanning electron microscopy (SEM), X-ray electron-probe microanalysis (EPMA), Electron backscatter diffraction (EBSD) and scanning confocal Raman spectroscopic imaging (SCμ-RSI). For a quantitative analysis of calcite, ACC and organic material we used a combination of X-ray diffractometry (XRD), thermogravimetry, (TG) and atomic absorption spectroscopy (AAS).

2. Material and methods

2.1. Animals

Helleria brevicoris Ebner, 1868, originally obtained from Alessandro Campanaro (Council for Agricultural Research and Economics, Research Centre for Plant Protection and Certification, Firenze, Italy) were kept and bred in a terrarium filled with wet soil at room temperature. They were fed with potatoes and dry leafs. For each analytical method, we studied the tergites of 2–7 animals in the intermoult stage. Animals were quickly killed by injecting 10–15 μm of 12% glutar aldehyde in 0.1 mol L^{-1} cacodylate buffer (pH 7.3).

2.2. Whole mount sample preparation and SEM

For SEM of surface structures of tergite cuticle, freshly killed *H. brevicornis* were dissected and fixed in a solution containing 1% glutaraldehyde in cacodylate buffer (pH 7.3) for 1 h. Samples were washed for 5 min in bi-distilled water and dehydrated in an ascending series of aqueous isopropanol solutions (30, 50, 70, 90, and 100% vol%) for 10 min each and critical point dried using a CPD 030 device (Bal-Tec, Liechtenstein). Whole mounts of dorsal cuticle were sputter-coated with gold/palladium in a Balzers MED 010 (Liechtenstein) and mounted on aluminium dishes using self-adhesive carbon pads and conductive glue. The whole mounts were analysed using a Zeiss DSM 962 SEM at an acceleration voltage of 20 kV using either a secondary or backscatter electron detector.

2.3. Sample preparation for scanning techniques

For the analysis of internal cuticle surfaces tergites were dissected in 100% methanol to avoid dissolution of amorphous calcium carbonate (Becker et al., 2003). Soft tissues were removed and the tergites were then washed in bi-distilled water for about 1–2 s to remove body fluids and then in 100% methanol for 25 s to remove the water (Seidl and Ziegler, 2012). Samples were air dried and either processed immediately or stored at −20 °C until further use.

To obtain sagittally fractured surfaces of tergites for field emission SEM (FESEM), air-dried samples were broken open using forceps. The samples were glued to aluminium holders using either superglue or sticky carbon pads and conductive glue, and rotary shadowed with a 3–4 nm thick layer of platinum at an angle of 45° using a BAF 300 (Balzers, Liechtenstein). For FESEM, EPMA, SCμ-RSI and EBSD such coated and uncoated samples were mounted on aluminium rods using superglue for microtome polishing. Polished surfaces were obtained by first cutting a sagittal plane with a diamond trimming knife (Diatome, Liechtenstein) and then with an ultra-type diamond knife (Diatome, Liechtenstein) cutting 15 thin sections each with a thickness of 95, 70, 45, 20, 10 and 5 nm (Fabritius et al., 2005). The samples were then coated with an about 5 nm thick layer of carbon (BAF 300). For EBSD, horizontal surfaces of tergite cuticle glued on aluminium dishes were microtome polished as well. Part of the sagittally polished samples for FESEM were edged by incubation in an aqueous MOPS buffered solution (10 mmol L^{-1}, pH 6.5) for 60 s. After washing three times for 10 min in isopropanol to remove the aqueous solution, samples were critical point dried and rotary shadowed with platinum in the same way as the fractured samples.

To investigate the spatial relation between organic and mineral phases using STEM and to improve the spatial resolution for EPMA, 60 nm thick sagittal thin sections were cut from non-demineralized air-dried cuticle samples using a 35° diamond knife and a Diatome Static Line II ionizer (Seidl and Ziegler, 2012). The sections were transferred to a carbon coated formvar film on 300 mesh copper grid, sandwiched by another coated grid and flattened by the mass (100 mN) of a polished brass-rod placed onto the sandwich. The sections were then coated with 4–8 nm thick carbon layer.

2.4. FE-SEM, STEM and EPMA

FE-SEM and STEM was performed using a Hitachi S-5200 (Hitachi High-Tech Corp., Tokyo, Japan) equipped with detectors for secondary and transmitted electrons at 4 kV and 30 kV acceleration voltage, respectively. Micrographs using backscattered electrons were recorded with a Hitachi SU 5000 FESEM. An EDAX Phoenix X-ray-detector system attached to the Hitachi S-5200 was used to record elemental maps at a pixel resolution of 512 × 400 and a dwell time of 200 μs per pixel leading to 88 full scans per hour. A full spectrum was recorded and stored for every pixel (spectral mapping). At each scan, spectra were integrated for every pixel allowing for standard-less background

corrected calculation of atomic ratios for selected regions. For bulk samples we used the ZAF mode and for thin sections the Mthin mode following the method of Zaluzec (1980) as implemented in the EDAX Genesis software (Ametek GmbH, Meerbusch, Germany).

2.5. Transmission electron microscopy (TEM) of decalcified thin sections

Air-dried tergites or freshly dissected tergites that were decalcified and fixed simultaneously for 20–30 days (Seidl and Ziegler, 2012) until complete decalcification using a solution containing 50 mmol L^{-1} EDTA, 2.5% glutaraldehyde, 2% paraformaldehyde, and 0.25 mol L^{-1} HEPES buffer (pH 7.8). The tergites were then washed 3 times in bi-distilled H_2O for 10 min each, post-fixed for 1 h in a solution containing 1% OsO_4 and 0.8% $K_4[Fe(CN)_6]$, washed again 3 times in bi-distilled H_2O for 10 min each, dehydrated in a graded series of isopropanol, block contrasted in a solution of 2% uranyl acetate in ethanol for 30 min, washed 3 times in ethanol, 2 times in acetone for approximately 4 min each, and embedded in EPON resin. 50 nm thick sagittal thin sections were cut using a Ultracut ultramicrotome (Leica, Austria) and a 45° diamond knife (Diatome). The sections were placed on copper grids, stained in 2% uranyl acetate solution for 10 min and 0.3% lead citrate solution for 1 min and analysed in a Jeol 1400 TEM and a Philips T400 with acceleration voltages of 120 and 80 kV, respectively.

2.6. X-ray powder diffractometry and quantitative analysis

High-resolution X-ray powder diffractometry was carried out in transmission geometry at room temperature (ground samples on Kapton foil) at beamline B2 at HASYLAB/DESY, Hamburg, Germany, at a wavelength of $\lambda = 0.47176$ Å (Knapp et al., 2004a; Knapp et al., 2004b). All data were converted to Cu Ka1 radiation wavelength ($\lambda = 1.54056$ Å). Relative mass fractions of calcite and quartz were calculated from the diffractograms using the Rietveld software FULLPROF Suite 2005 (Rodriguez-Carvajal, 1990). For quantitative Rietveld analyses, the air-dried tergite samples were mixed with crystalline quartz (SiO_2) in a 5:1 = *w:w* ratio, followed by thorough grinding. For more details including an estimation of the accuracy of the method see Neues et al. (2007). The amount of magnesium in calcite substituting for calcium was determined by analysing the shift of the diffraction peak (Goldsmith and Graf, 1958). Atomic absorption spectroscopy (AAS) was used to measure the calcium and magnesium content using a Unicam 939 AAS instrument. Thermogravimetric analysis was performed with a Netzsch STA 409 instrument in a dynamic oxygen atmosphere (50 mL min^{-1}) at a heating rate of 3 K min^{-1}. Calculations for the determination of the calcite and ACC content from combined elemental analysis and X-ray powder diffractometry are described elsewhere (Becker et al., 2005). We assumed that the difference between the total calcium content determined by AAS and the calcium content in calcium carbonate was due to the ACP. The content of ACP was calculated using the stoichiometry of hydroxyapatite, $Ca_5(PO_4)_3OH$.

2.7. Scanning confocal micro Raman spectroscopic imaging (SCμ-RSI)

SCμ-RSI was performed on sagittal plains of tergite sections to allocate the distribution of calcite, amorphous calcium carbonate, organic material and phosphate. A WiTec scanning confocal Raman microscope (Alpha-300R, WiTec GmbH, Ulm, Germany) was used, operating with an NdYag laser at 532 nm at an intensity of 8 mW, a Nikon (50, air, NA = 0.8) objective lens and a piezo- driven scan stage. The spatial resolution was 300 nm in the lateral × and y axes and about 500 nm in the z-axis. The spectral resolution was about 3 cm^{-1} for a full spectrum ranging from 0 to 3750 cm^{-1} using a diffraction grating of 600 grooves per cm. The Rayleigh peak was suppressed using a holographic edge filter. The incident light was polarized either by 0 (P0) or 90° (P90) in relation to the x-scan axis. All spectra were recorded with the WiTec-Control acquisition software (WiTec GmbH, Ulm, Germany). Samples were imaged with a raster of 9 pixels per 1 μm^2. At each pixel a full Raman spectrum was recorded with an integration time of 0.5 s. WiTec-Project software (Version 2_08, WiTec GmbH) (Schmidt et al., 2005). For each pixel we integrated the band for the external (lattice) vibration between 260 and 310 cm^{-1} (∑Calcite) and that of the band for symmetric stretching vibration of carbonate between 1070 and 1100 cm^{-1} (∑Carbonate) using the WiTec-Project software. The C–H and CH_2 stretching vibration between 2800 and 3100 cm^{-1} (∑Organic) [chitin and protein] and the phosphate vibration between 930 and 980 cm^{-1} (∑Phosphate) were also integrated. For imaging of the calcite, total carbonate, organic material and phosphate distributions the integrated values were plotted in x–y coordinates after intensity coding in red, orange, green and cyan, respectively. A synthetic calcite single crystal, amorphous calcium carbonate from the sternal deposits of *Porcellio scaber*, chitin from purified crab shell (Sigma– Aldrich), bovine serum albumin (Sigma–Aldrich) as a protein standard, hydroxyapatite, and amorphous calcium phosphate (ACP) from the pleoventral deposits of *Tylos europaeus* (Ziegler, 2003) were used as references as published previously (Ruangchai et al., 2013).

2.8. Electron backscatter diffraction (EBSD)

EBSD measurements were carried out by Dr. Erika Griesshaber (Department of Earth and Environmental Sciences and GeoBioCenter at the LMU Munich), using a field emission SEM SU5000 equipped with a Nordlys II EBSD detector and AZTec and CHANNEL 5 HKL software. The SEM was operated between 12 and 20 kV. Diffraction data gained from EBSD are processed for (a) depicting characteristics of the microstructure of the calcite layer with band contrast measurement images, (b) crystal orientation patterns (shown with color-coded orientation maps), (c) the texture of calcite (given with pole figures visualizing individual data points of the corresponding orientation map) and (d) crystal co-orientation strengths (calculated from c- and a-axes pole density distributions). Grey scaled EBSD band contrast images depict the signal strength in each individual measurement point. The signal is high when a crystal is detected (depicted in the map with light grey), whereas it is weak or absent when amorphous mineral or a polymer is scanned, or when minute crystallites overlap, so that the orientation cannot be resolved automatically (dark/black) with the used EBSD software (Ernst et al., 2020b).

3.0. Results

3.1. Surface structures

Fig. 1A shows *H. brevicornis* in its unrolled posture. Tergites 2–7 have an anterior part, where the dorsal surface appears smooth and slides under the preceding tergite when the animal unrolls, and a posterior part that is always exposed to the environment (Fig. 1B). At the posterior margin a row of large rectangular scales covers the gap to the next tergite (Fig. B-D). The tergites are covered with two types of pectinate scales with either short or long comb-teeth pointing posteriorly (Fig. 1D-F and Regions bearing scales with long comb teeth and those bearing short ones are separated from each other (Fig. S1). About 6 scale rows at the posterior margin point in the opposite, anterior direction with partially connected comb teeth (Fig. 1F). The posterior part of the tergites bears two types of sensilla that occur only on regions with scales having long comb teeth (Fig. 2 and Fig. S1). One type varies in length and can be longer than 50 μm. It consists of a long socket structure covering an inner sensory hair (Fig. 2B-D). Large sensilla are lacking in the anterior part of the tergites, resulting in a smoother appearance (Fig. 1B). The second type occurs on both parts and is hidden in small cavities (Fig. 2A, E, F). It consists of a short sensory-seta within a short socket structure (Fig. 2D, E). The base of both types of sensilla are covered by 1–3 distinct outer scales (Fig. 2D, E). The cuticle of both, the sockets and inner sensory seta branch into many filaments giving the

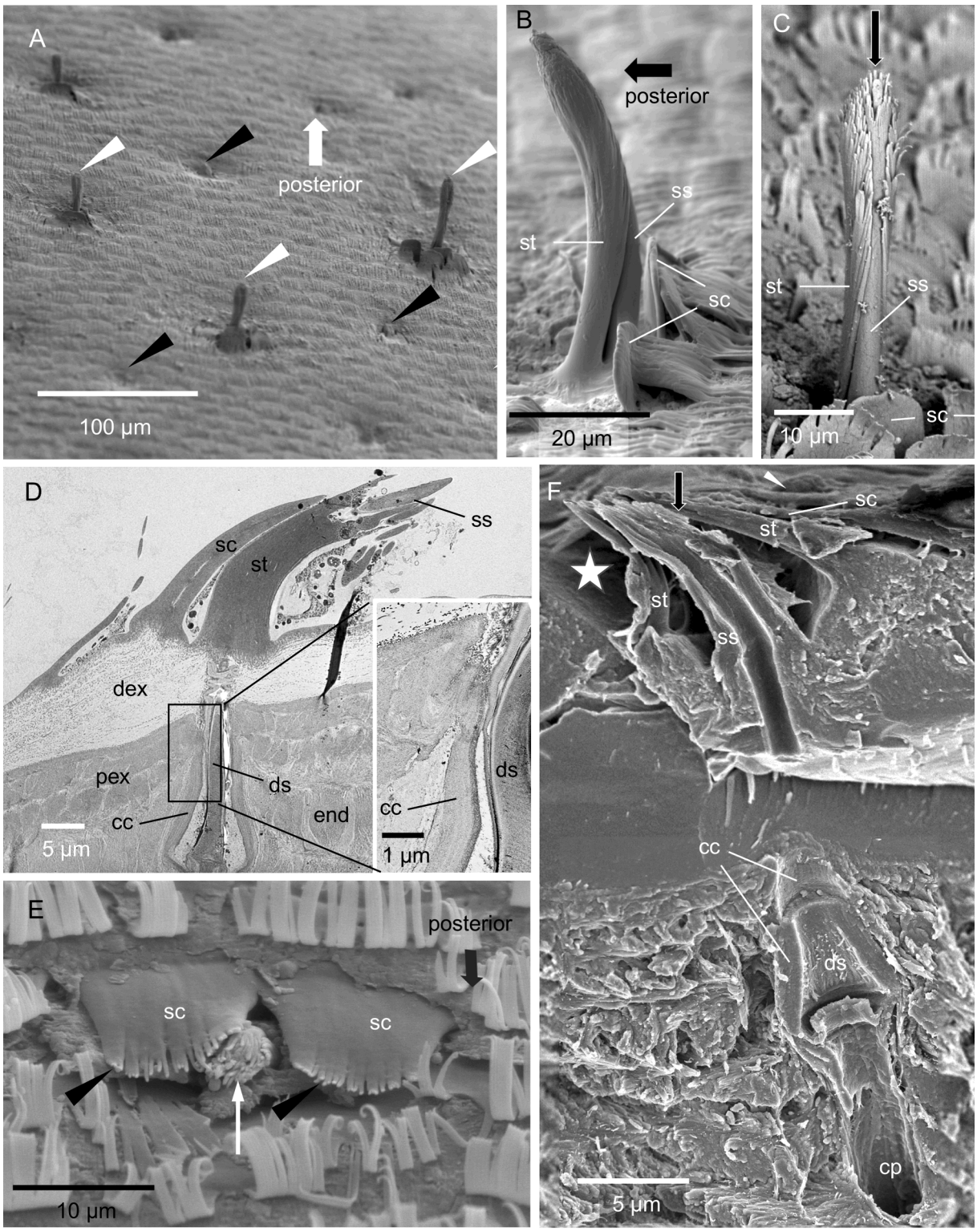

Fig. 2. The structure of sensilla on the tergites. A) The tergites carry large (white arrowheads) and small sensilla (black arrowheads), B, C) SEM micrographs of large sensilla consisting of an inner sensory seta (ss) covered by a socked structure (st) and two scales (sc). The arrow in C points to an apical pore. D) TEM micrograph of a sagittal plane through a large sensillum. Within the cuticle, it forms a dendritic sheath (ds) with a cone shaped proximal end. A cone shaped structure (cc) of the proximal exocuticle (pex) projects into the endocuticle (insert); dex, distal exocuticle; end, endocuticle. E) A small sensillum (white arrow) covered by two scales. F) SEM micrograph of a fracture through a small sensillum. Small sensilla have the same inner structure as the large ones. The socket and the sensory hair are positioned in a cavity of the cuticle (white star); cp, pore for the traversal of the dendrites.

sensilla a brush-like appearance (Fig. 2C, E, F and Fig. S2). The tip of the sensory seta has a pore that is mostly covered by the apical filaments (Fig. 2C, E and Fig. S2) and can be seen well in fractures through a sensillum (Fig. 2F). In both types the sensory hair projects deep into the cuticle where it ends in a cone shaped dendritic sheath (Fig. 2D, F). The dendritic sheath is surrounded by an, as well cone-shaped, structure of outer stacks of the proximal exocuticle. The outer parts of the sensilla consist of epicuticle only (Fig. 2D). The sensory setae have a central

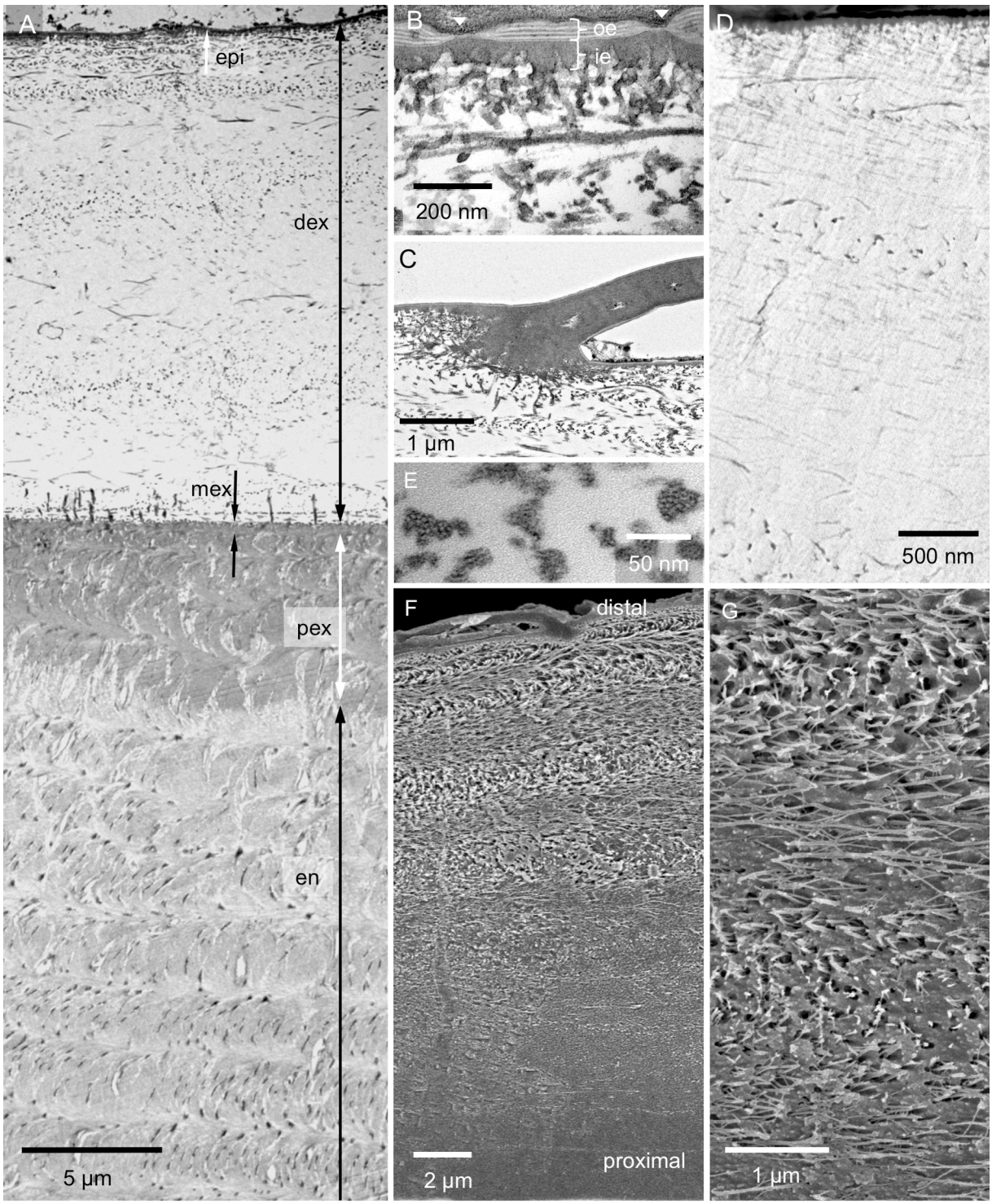

Fig. 3. The internal structure of the epicuticle and the distal exocuticle of the tergite; A-C and E: TEM micrographs; D: STEM micrograph of a non-decalcified thin section trough the distal exocuticle; F and G: SEM micrographs. A) Overview of the tergite cuticle depicting the epicuticle (epi), distal (dex) and proximal exocuticle (pex) and the endocuticle. B) The epicuticle consists of an outer (oe) and an inner epicuticle (ie). The outer epicuticle contains densely stained and light layers. C) Near and below scales the epicuticle becomes thicker. D) Non-decalcified sections show that the mineral (bright) is situated between scarcely distributed fibres (dark lines and dots); note that the grey levels are reversed. E) The fibres consist of bundles of chitin fibrils (arrowhead) within a densely stained matrix. F, G) Micrographs of sagittally polished and edged surfaces show the twisted plywood arrangement of fibres within dex. F) Etching at pH 6 results in a graded dissolution of mineral from distal to proximal. G) Mineral dissolves preferentially around the fibres.

channel and a pore through the endocuticle through which the dendrites of the sensory cells can pass (Fig. 2F)

3.2. The structure of the epicuticle

The cuticle consists of an outermost distal epicuticle, exocuticle, and an endocuticle (Fig. 3A, B). The epicuticle is about 150 nm thick. It has an about 50 nm thick outer and a 100 nm thick inner epicuticle (3B). The thickness of the outer epicuticle varies and occasionally notches can be observed, in which the thickness is reduced to about 15 nm. The outer epicuticle contains between 1 and 5 densely stained layers which are bordered by light layers (Fig. 3B). The dense layers have been designated as waxy layers (Compère, 1990). The inner epicuticle is about 100 nm thick and has a jagged proximal edge. At the base of epicuticular scales (Fig. 3C) as below the sensilla (Fig. 2C) the inner epicuticle is much thicker than in other regions, likely forming an anchoring together with fibres of the subjacent exocuticle.

3.3. The structure of the exocuticle

The exocuticle consists of a distinct distal 20–30 μm thick layer, a proximal about 5 μm thick layer and middle layer that is 500 nm thick (Fig. 3A). The distribution of organic fibres and mineral in the distal exocuticle can be well observed in thin sections from non-demineralized samples (Fig. 3D). Individual fibres are far apart up to 300 nm, with the space between them filled with calcium carbonate. TEM images reveal that the fibres are between 10 and 50 nm thick and that the cross-sections have an irregular shape. They consist of typically 5–20 unstained 3 nm thick chitin fibrils embedded in a likely proteinaceous matrix (Fig. 3E). The fibres of the distal exocuticle form a twisted plywood structure of mostly 6–10 stacks (Fig. 3A, G). The most distal stacks have a higher density of fibres. These are about 1 μm thick and always thinner than the more proximal stacks that can be more than 5 μm thick (Fig. 3A, F). During etching at pH 6.5, mineral of the outer region of the distal exocuticle dissolves better than proximally (Fig. 3F) and mineral dissolves particularly well around the fibres (Fig. 3G).

Samples of the distal exocuticle that were fractured in the native non-demineralized state have smooth surfaces interrupted by polyhedral structures (Fig. 4A). The mineral is composed of granules about 20–30 nm in diameter (Fig. 4B). The polyhedral structures decrease in size distally (Fig. 4A). Besides the polyhedral and smooth surfaces, we observe regularly spaced about 600 nm thick vertical columns of mineral (Fig. 4C). Samples that were fractured almost horizontally disclose that these structures form walls with a polygonal pattern. Fan-shaped mineral structures radiate from these in a horizontal direction (Fig. 4C, D). TEM micrographs of sections from decalcified and resin embedded samples reveal that the walls contain organic fibre-like and globular material of irregular distribution (Fig. 4E, F), structurally distinct from the chitin-protein fibres of the twisted plywood in the distal exocuticle. Samples cut nearly horizontally show that the organic material within the walls have a polygonal distribution (Fig. 4G).

The organisation of the organic phase changes abruptly from a sparse distribution of fibres in the distal exocuticle to a dense distribution of individual fibrils of all underlying stacks (Fig. 5A, B). In all layers the fibres are oriented in a planer twisted plywood. A median layer, between the distal and proximal exocuticle, consists of 1 or 2 stacks, which together are only about 300 nm thick and are more densely stained than the stacks below. The proximal exocuticle consists of 3–4 stacks (Fig. 3A and 5A). Distal stacks are about 1 μm and the most proximal stack is 2–3 μm thick (Fig. 3A and 5A). Pore canals within the proximal exocuticle are branched, interconnected and contain fibrils following the direction of the canals (Fig. 5B, C). They terminate below the median layer of the exocuticle and are thus not within the distal exocuticle (Fig. 5B, D). Sections of non-demineralised cuticle show that within the median and proximal exocuticle fibrils are individually surrounded by mineral (Fig. 5D-F). Cleaved surfaces of the exocuticle reveal a distinct border between its distal and proximal part (Fig. 5G) The dry median and proximal exocuticle fracture partly between fibrils making the twisted plywood arrangement of the fibrils visible, in contrast to the fractured surface of the distal exocuticle, which is not influenced by the fibre orientation (Fig. 4A and 5G).

3.4. The structure of the endocuticle

The border between the proximal exocuticle and the endocuticle is very distinct in TEM micrographs of decalcified samples since the fibrils in the proximal exocuticle stain darker than in the endocuticle (Fig. 5A). The endocuticle is about 50 μm thick. In the distal part of the endocuticle, stacks have more or less the same thickness between 5 and 3 μm (Fig. 3A, Fig. 5A, Fig. 6A, B and Fig. S3). Pore canals in the endocuticle run perpendicular to the cuticle surface and contain vertical fibrils, which form twisted ribbons that follow the twist of horizontal fibrils (Fig. 6A). Distal regions of the endocuticle cleave in a similar way as the proximal exocuticle (Fig. 6B). Sections of non-demineralised endocuticle show that the fibrils, as in the proximal exocuticle, are individually surrounded by mineral (Fig. 6C). In the proximal region, the size of the stacks decline from 2 μm to a few hundred nm (Fig. 6B, D and Fig. S3). In the proximal region, the fracture surfaces appear spiny, since more fracture surfaces run along the fibrils than through them. This leads to a regular pattern of spines and holes in the surface (Fig. 6D, E). Large pore canals are lacking in proximal stacks and are replaced by a different type of canal-like structures. They are about 50 nm thick and the distances between them are about 500 nm or less. They have a wall of smooth appearance and are devoid of fibrils (Fig. 6D, E).

3.5. Content of calcite, ACC, magnesium and organic material

Quantitative data on the composition of the tergite cuticle were obtained by combining results from atomic absorption spectroscopy (AAS), thermogravimetry (TG), and X-ray powder diffraction (XRD) (Fig. 7A) and are summarized in Table 1. The values in Table 1 refer to the dry mass of the sample. A total calcium amount of 32.4 wt% and a total magnesium amount of 0.55 wt% was determined by AAS. The amount of calcite of ca. 18 wt% was determined by XRD using a quarz standard (Fig. 7A). The contents of organic material (14%), the total mineral content (86%), and content of calcium carbonate (77%) were determined by TG; and the content of ACP was estimated to be 4% (Fig. 7B).

3.6. Element distribution

Elemental mapping shows that the calcium content in a distal layer of the exocuticle is higher than in the proximal ones and within the endocuticle. At the proximal side, a layer about a quarter the thickness of the endocuticle has a lower calcium concentration than in the rest of the endocuticle (Fig. 8A). The phosphorus concentration is high in the proximal exocuticle and a distal part of the endocuticle forming two layers with higher phosphorus content. Magnesium appears evenly distributed. Fig. 8B shows elemental maps from a thin section through the region around the median exocuticle. The distal exocuticle, the thin median exocuticle and the proximal exocuticle can be well distinguished. The maps show that the region of high calcium concentrations is limited to the distal exocuticle and that within the pore canals the calcium content is higher than in the surrounding areas. The magnesium content is somewhat higher in the distal exocuticle as compared to the subjacent layers. The molar ratios of magnesium and phosphorus are 3.1 and 0.9 mol per 100 mol of calcium in the distal exocuticle, 3.6 and 5.7 mol per 100 mol of calcium in the median exocuticle and 3.4 and 5.9 mol per 100 mol of calcium in the proximal exocuticle. Fig. 8C shows elemental maps of the cuticle near a sensillum. Distally, the mineral in the cuticle around the sensory channel has a high phosphorus content.

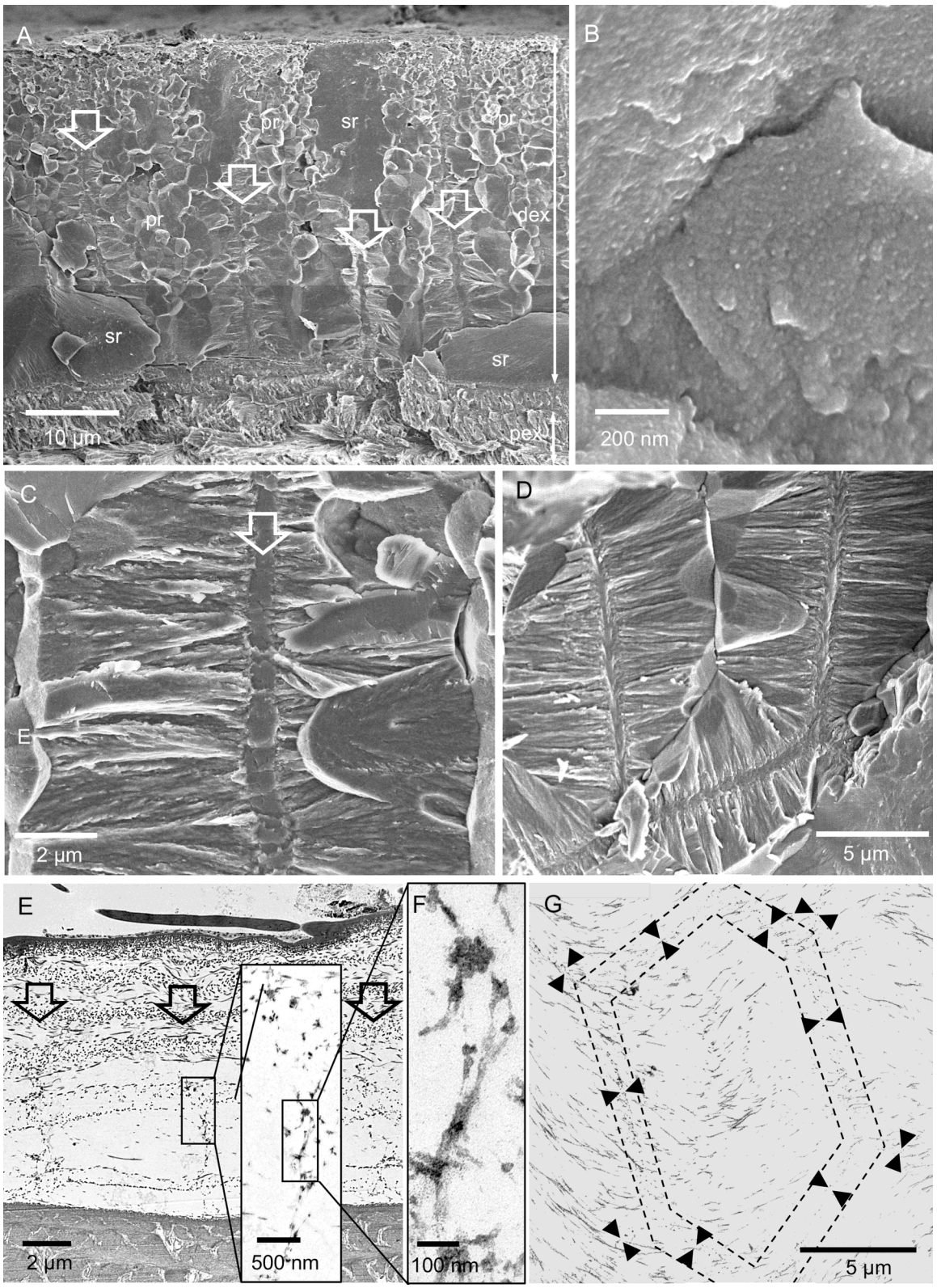

Fig. 4. The structure of the mineral phase in a fracture sample of the distal exocuticle. A-D: FE-SEM micrographs. A) Overview of the distal exocuticle (dex) and part of the proximal exocuticle (pex). In dex regions with polyhedral structures (pr) alternate with smooth regions (sr). Within, the polyhedral regions are vertically oriented sheet-shaped structures of mineral (white arrows). B) The mineral phase consists of particles about 20 nm in diameter. C) Detail of a fracture through a sheet shaped structure. Mineral fibres extend radially outwards from the sheets. D) An almost horizontal fracture through dex shows that the sheets surround prism like areas. E-G) TEM micrographs of organic material within dex, depicting organic material within the sheets. E) Overview of dex from a sagittal section. The black arrows mark vertically oriented organic structures. The inset shows a detail from the area marked with a rectangle. F) A detail from the inset in E shows discontinuous globular and filamentous structures. G) Micrograph of a horizontally oriented sections through dex. The organic matrix of the mineral sheets forms a polygonal pattern marked by the black arrowheads between the two dashed polygons. Fig. 4C from Fabritius et al. (2016) with permission.

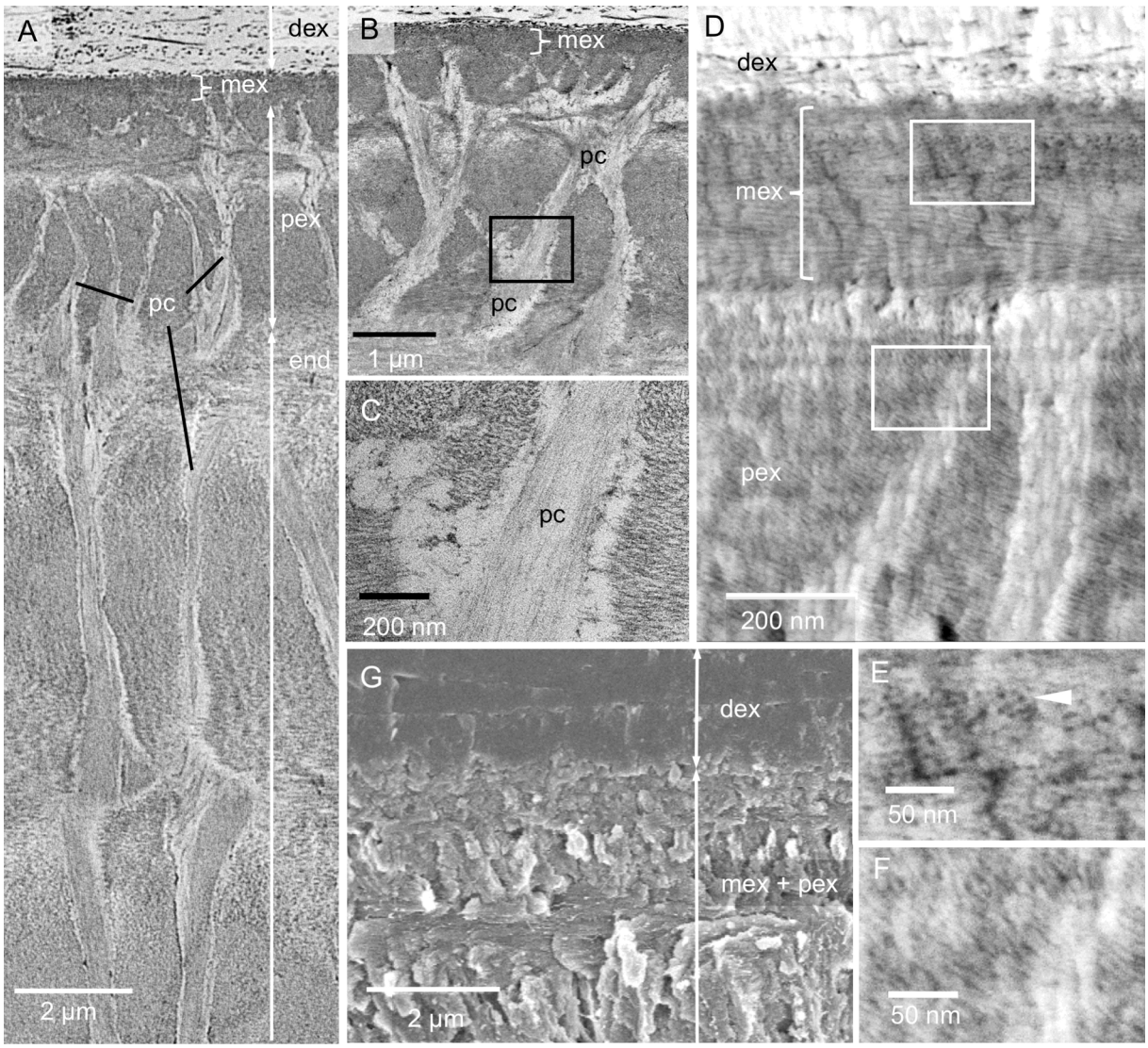

Fig. 5. The structure of the proximal exocuticle. A-C: TEM micrographs. A) Overview showing the a median exocuticular layer (mex) underneath the distal exocuticle (dex) the proximal exocuticle (pex) and distal layers of the endocuticle (end); pc, pore canals. B) Pore canals form branches and end underneath mex. C) Detail from the region marked with a rectangle in B showing filaments inside the pore canals. D-F) STEM micrographs of non-demineralized thin-sections. Note that the grey levels are reversed so that mineral appears bright and organic fibrils dark. D) In mex fibrils form 1–2 stacks and the mineral content is lower than in dex and pex. Pore canals have a high mineral content. E, F) Details from a region in mex and pex marked by rectangles in D. Each fibril within mex and pex is individually surrounded by mineral. G) Fractured surface through mex and pex.

3.7. The distribution of mineral and organic phases

The Raman spectral maps (SCμ-RSI) (Fig. 9A) and accumulated spectra from 3 different regions (Fig. 9B) show the distribution of calcite, the total amount of calcium carbonate, the organic phase of chitin and protein, and the distribution of phosphate. The averaged spectrum of the calcite containing area (Fig. 9Ba) has bands at 158 cm^{-1} and 280 cm^{-1} characteristics for the calcite lattice vibrations and a narrow band at 1088 cm^{-1} characteristic for CO_3-stretching vibrations. Calcite is restricted to a distal layer, likely corresponding to the distal exocuticle, were the amounts of organic material and phosphorus are near or below the detection limit (Fig. 9Ba). There is a sharp and straight border between the distal layer of calcite and the more proximal layers (Fig. 9A and 5D). No calcite was found below the distal exocuticle. Here the $CaCO_3$ content is considerably lower than in the distal exocuticle. The mineral consists of ACC, which is indicated by a wide band between 100 cm^{-1} and 300 cm^{-1} replacing the bands for the calcite lattice vibrations, and by widening of the band for CO_3– stretching vibration and a shift from 1088 to 1083 cm^{-1} (Fig. 9B). The presence of organic material within the region containing ACC is indicated by a band for C–H stretching vibrations between 2800 cm^{-1} and 3020 cm^{-1} (Fig. 9A, Bb, Bc). The highest amount of organic material is found in an unmineralized layer at the proximal side of the cuticle, representing a membranous layer (Fig. 9A). A band at 960 cm^{-1} indicates the presence of phosphate in the distal side of the ACC containing region (Fig. 9A, Bb). This band is not visible in the calcite containing distal exocuticle and very low at the proximal side of the cuticle (Fig. 9A, Ba, Bc). The signal intensity for the Raman calcite and carbonate bands depends on the orientation of the calcite-crystal lattice with respect to the polarisation of the incident light (Fig. 9A, C). Fig. 9C shows maps for calcite and carbonate at 0° and 90° polarisation and corresponding colour-coded maps for the intensity ratio CR = ∑carbonate/∑calcite. The maps show areas of calcite up to 25 µm in size with different crystallographic orientation. Fig. 9D shows a cluster analysis in which domains with similar spectra have the same colour. The individual CR values of these clusters change by factors between 1 and more than 5 when the polarisation of the incident light is

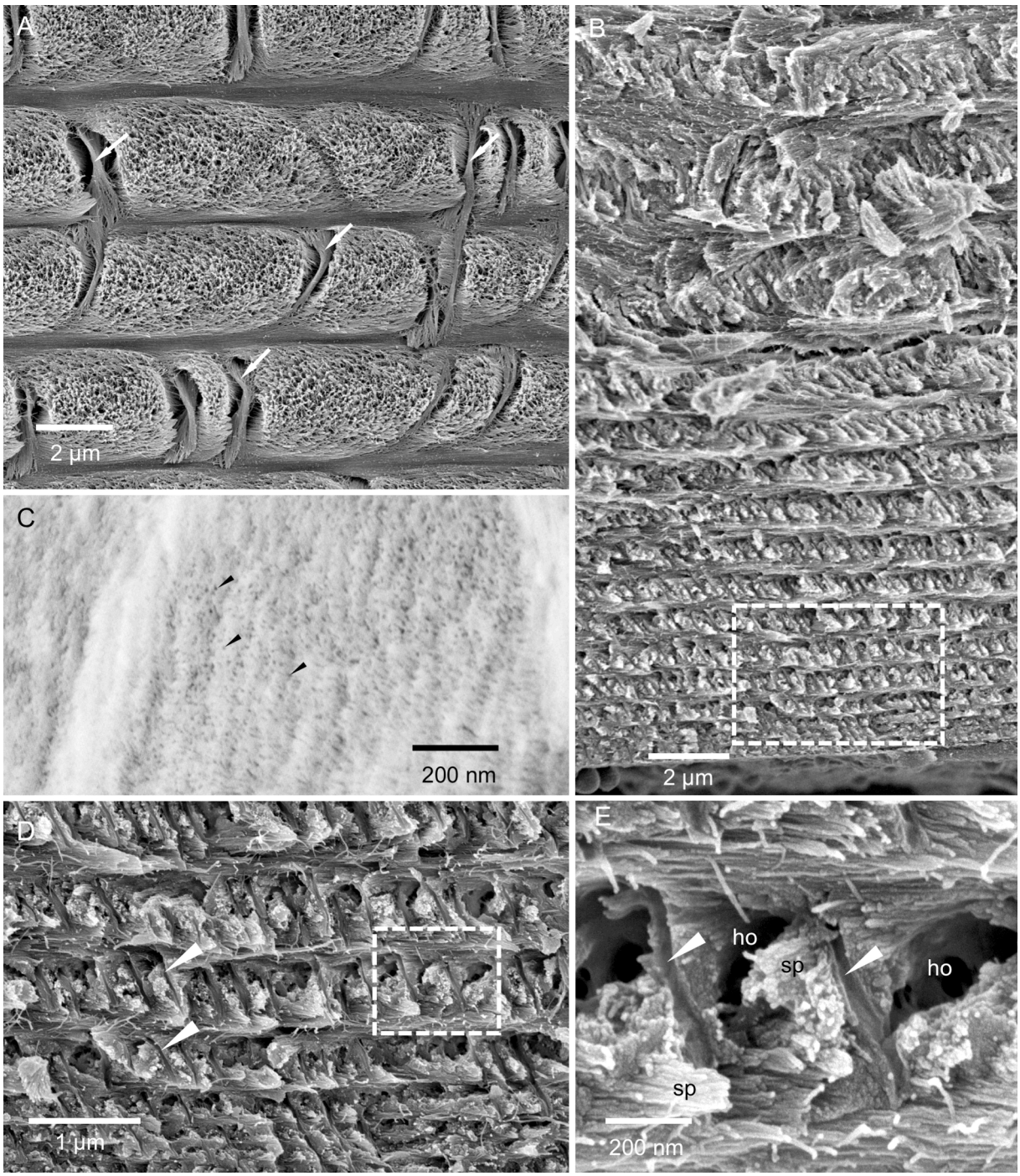

Fig. 6. The structure of the endocuticle. A) FE-SEM micrograph of distal stacks of the endocuticle from a polished and etched sample, showing twisted plywood arrangement of fibrils. Pore canals contain a twisted ribbon of fibrils (white arrows). B) FE-SEM micrograph of a fractured surface of the proximal side of the endocuticle. Stack thickness decreases towards the proximal side. C) STEM-micrograph from a thin section of non-demineralized cuticle. Note that the grey levels are reversed so that mineral appears bright and organic fibrils dark. Fibrils (black arrowheads) are individually surrounded by mineral. D) Detail from B, and E) detail from D. Proximally the cuticle fractures preferentially along the fibrils leading to spines (sp) and holes (ho) within the surface. The cuticle contains thin pore canals with a smooth surface (white arrowheads).

switched by 90° indicating variations in the orientation between clusters (Fig. 9E). At an orientation of 45° with respect to polarisation of the incident light CR is about 0.5 and higher angles result in higher CR values (Seidl et al., 2012). Most clusters have CR values below 0.5 (Fig. 9E) indicating an orientation preference of the c-axes parallel to the surface of the sample (Seidl et al., 2012).

3.8. The calcite crystal orientation pattern

EBSD measurements were performed on four *H. brevicornis* samples, three tangential and one sagittal section (Figs. 10-13, Figs. S4-S7). A major feature of the calcite layer is the presence of a network of polygons, which are about 20 µm in size, best observable in the distal region of the calcite layer (Figs. 10 and 11). In the following we distinguish between peripheral walls of the polygons and the polygonal space

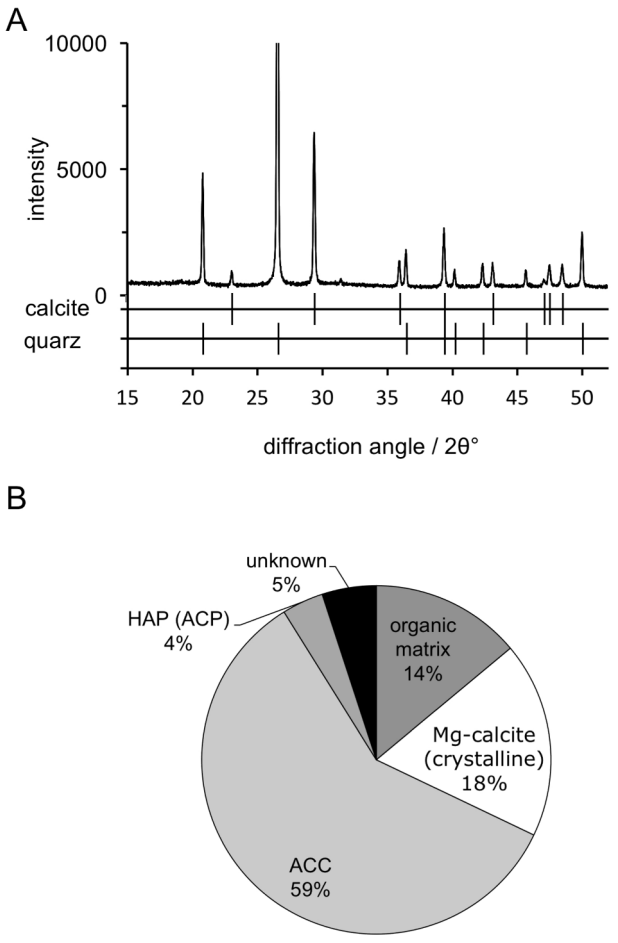

Fig. 7. A) X-ray powder diffractogram of the tergite cuticle mixed 5:1 with quartz. B) Schematic representation of the relative composition of mineral phases and organic material in the anterior and posterior tergite cuticle in their dry state.

within these walls. When based on calcite orientation, we see that: (i) small crystals in distal regions of the calcite layer that fill the polygonal space between the walls (Fig. 10B, Fig. 11A B, Fig. 12A, Fig. 13 and Fig. S4A, B, E) and (ii) the presence of large, interlinked, co-oriented crystals at proximal regions of the calcite layer (Fig. 10A, C, Fig. 11A and Fig. 12A).

Distally the walls of the polygons form mostly hexagons with a regular geometry (Fig. 10B, Fig. 11A, B, Figs. S5 and S6). Most of the small calcite crystals have similar orientations to the calcite in the nearby polygon walls. Calcite in the polygon walls have a higher co-orientation than the small crystals within the polygonal space. These polygonal walls and the nearby small crystals form larger co-oriented crystal-domains as indicated by similar colors (Fig. 11A and Fig. 13B, D). In addition, for about one third of the polygons in the distal region of the calcite layer, the polygonal space contains small to minute crystals, which orientation is different to the orientation of calcite within the polygon walls (Fig. 10B and S4). The pole figure (Fig. S4F) visualizes that these small crystals are less co-oriented in comparison the large co-oriented crystal-domains (compare the pole figures shown in Fig. S4D and S4F). Black regions in the EBSD maps around those minute crystals contain calcite as well as shown by the Raman spectroscopic and elemental maps (Fig. 8A and 9A, C). However, mineral is lacking at regularly distributed regions at the very distal region of the calcite layer (Fig. 12C and Fig. S7). These regions correspond to the sites underneath epicuticular scales, that contain thick proximal epicuticle (Fig. 3C). In the proximal region, which contain large calcite crystals, the shape of the polygons is less regular than in the distal region (Fig. 11C, D). The polygon walls within these large crystals are less visible than in the co-oriented calcite-domains in the distal region of the calcite layer (Fig. 12C, 11A, B), but can be readily observed with BSE when the calcite in the walls is denser than in the surrounding calcite (Fig. 12C and Fig. S7). The large proximal calcite crystals comprise about two third of the calcite layer (Fig. 12A, B, D).

The domains of small calcite crystals and the calcite crystallites in the calcite layer do not have a sharp texture (see pole figures in Figs. 10 and 12A). However, the calcite c-axes are oriented parallel to the cuticle surface with only little preference to the lateral sides of the animal (Fig. 10A, 12A and Fig. S4A, C, D). There appears to be no systematic relationship between microstructural and texture characteristics of the calcite layer (Fig. 10). It is striking that the co-oriented crystal domains and the large crystals do not follow the shape and the pattern of the polygons. Instead, the polygon walls are always within the co-oriented calcite units and have a similar orientation as the surrounding calcite. The distribution pattern of calcite orientation is thus linked to the polygon walls rather than to the polygon pattern itself. Within most polygonal spaces calcite has more than one, mostly 3 to 4 common orientations (Fig. 11B, D). Units with co-oriented calcite, vary considerably in shape and size and can even span across the walls of two or more polygons (Fig. 13B, D). In sections through the calcite layer, the size of co-oriented calcite unit profiles range from a few micrometers only to up to 60 μm with a mean size of 17.10 ± 8.2 μm (mean ± standard deviation, N = 100).

4. Discussion

4.1. Surface structures and epicuticle

There are a number of similarities and differences between the surfaces of the tergites of *H. brevicornis* and the beach isopod *T. europaeus*. In part, these differences can be attributed to differences in the substrate in which the species burrow. In *T. europaeus* micro-tubercles are abundant on the posterior part of the tergite cuticle that may prevent adhesion of moist sand during burrowing (Seidl et al., 2011). The absence of such tubercles on the tergites of *H. brevicornis* probably makes it more difficult for a predator to grasp and unroll the animal in the rolled-up posture. The sensilla on the tergites have the typical characteristics of tricorn sensilla. They are the most abundant sensilla found exclusively in terrestrial isopods (Holdich, 1984; Holdich and Lincoln, 1974; Price and Holdich, 1980; Schmalfuss, 1978). The large tricorn-type sensilla of

Table 1
Composition of the tergite cuticle of *Helleria brevicornis* (in wt% if no other unit is given). ACP was assumed as having the same stoichiometry like hydroxyapatite, $Ca_5(PO_4)_3OH$. The column "total mass" denotes the sum of Mg-calcite, ACC, organic matrix, and ACP. Formulae for calculations are described in details elsewhere (Becker et al., 2005).

Ca (AAS)	Mg (AAS)	Organic matrix (TG)	Total mineral Content (TG)	$CaCO_3$ (TG)	Crystalline Mg-calcite (XRD)	ACC (XRD and TG)	ACC/calcite (wt %/wt%)
32.4	0.55	13.9	86.1	77.19	18.2	59.0	3.25
Mg/Ca (wt %/wt%)	Mg:Ca (mol/mol)	$MgCO_3$ in Mg-calcite (mol%)	Mg in Mg-calcite based on sample wt	Mg not in Mg-calcite	Ca not in $CaCO_3$	ACP	total mass
0.017	0.028	1.02	0.25	0.51	1.35	3.85	95.0

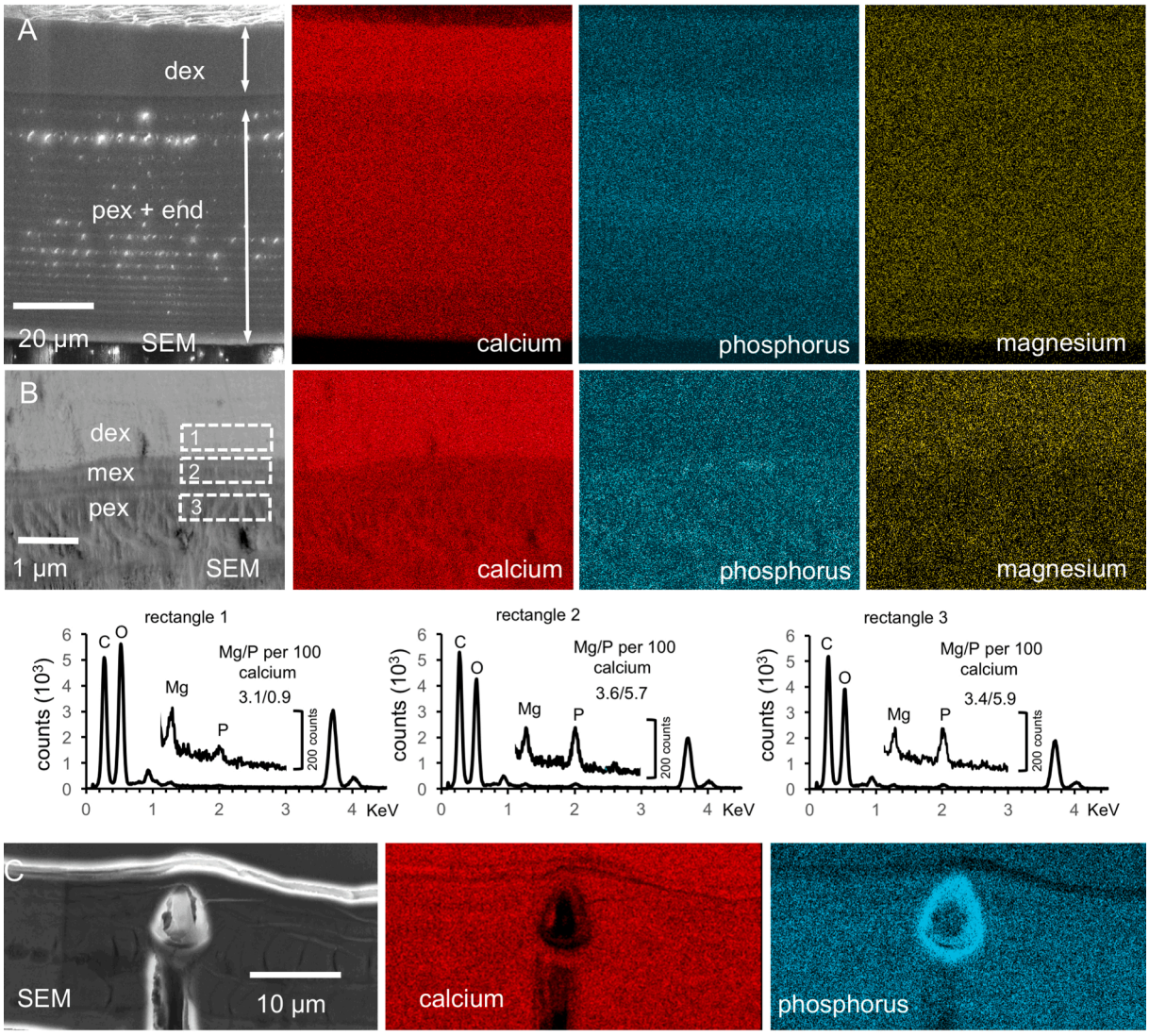

Fig. 8. Elemental composition of the tergite cuticle. A) SEM micrograph and elemental maps from a polished bulk sample. Calcite content is higher in the distal exocuticle (dex) than in the proximal exocuticle and endocuticle (dex + pex). Phosphorus concentration is high in a region below dex. Magnesium appears more or less evenly distributed. Note the presence of thin proximal unmineralized layer in the SEM micrograph that corresponds to a membraneous layer. B) STEM micrograph, elemental maps and average spectra from the regions marked with dashed rectangles. Calcium and magnesium is highest in dex. C) Elemental maps of the tergite cuticle at a sensillum. Distally around the channel for the dendrites the phosphorus content is high.

H. brevicornis likely respond to external mechanical as well as chemical stimuli as suggested for other terrestrial isopods (Hatanaka, 1989; Wood et al., 2017; Ziegler and Altner, 1995). Sensilla with a single apical pore are regarded as contact chemo-receptors (Altner and Prillinger, 1980). The brush-like structure of the small and large sensilla increase the surface at their tip likely facilitating wetting by capillary forces. This may improve access of chemical substances to the pore of the sensillum and is possibly an adaptation to the soil habitat of the species. The small tricorn-type sensilla hidden inside cavities are likely protected from external mechanical stimuli, however, they may respond to bending of the cuticle upon external and internal forces in addition to chemical stimuli. Such small sensilla and sensilla with brushed tips have not been found on the tergite surface of *T. europaeus*. Pectinate scales occur in *T. europaeus* as well and have also been found in the marine isopods *Jaera marina* and *Limnoria lignorum* (Powell and Halcrow, 1982; Seidl et al., 2011). The scales that point to the anterior instead to the posterior direction near the posterior margin on the tergite of *H. brevicornis* may help prevent soil particles from getting between the tergites. So far, such scales have not been reported from any other isopod species.

The epicuticle is thought to be the main barrier against evaporative water loss through the cuticle of terrestrial isopods (Compère, 1990; Hadley and Warburg, 1986). Dense layers within outer epicuticle are called “waxy layers” because it stains with osmium tetroxide and can be dissolved in a hot chloroform/methanol mixture. They were suggested to act as a surface waterproofing barrier (Compère, 1990). Therefore, one would expect that the number of dense layers correlate with the dryness of the animal’s habitat. This, however, appears not to be the case. Both *H. reaumuri*, which lives in leaf litter and humus, and *T. europaeus*, which burrows in moist sand, are not exposed to dry conditions, but the number of dense layers is up to five for *H. brevicornis* and only one for *T. europaeus*. A recent study on the tergites of *Hemilepistus reaumuri*, which lives in desert habitats and is exposed to high temperatures during the day in summer, has shown that the outer epicuticle contains only a single dense layer (Ernst et al., 2020b). Furthermore, a comparative study showed no differences in the number of dense layers within the outer epicuticle between troglobitic and non-troglobitic species, although the air in caves is nearly saturated with water (Vittori and Štrus, 2014). Therefore, Vittori and Štrus (2014) suggested that multiple layers within the epicuticle might be related to the presence of epibionts, support of epicuticular surface structures or

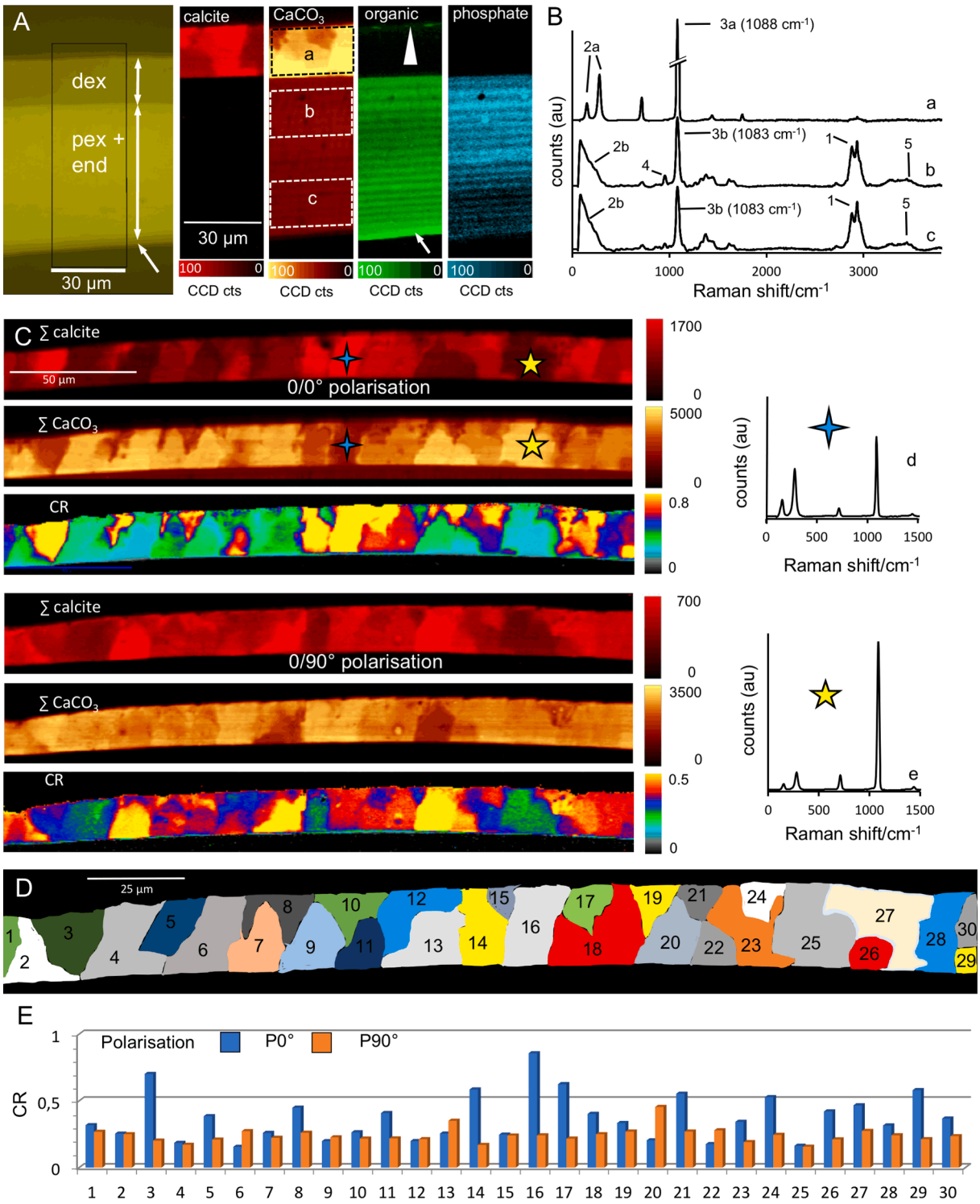

Fig. 9. Raman spectral images and spectra and from tergites of *Helleria brevicornis*. (A) Distribution of calcite, total amount of calcium carbonate ($CaCO_3$), organic matrix and phosphate. Calcite occurs in the distal exocuticle (dex) only, whereas calcium carbonate occurs within the whole exo- and endocuticle. Organic material is abundant within the epicuticle (arrowhead) and the proximal exo- (pex) and endocuticle (end). Within dex organic material is below the detection limit. The membranous layer (arrow) is devoid of mineral. B) Average spectra of dex (a), pex (b) and the end (c). Bands for C–H stretching vibration (1) occur between 2800 and 3020 cm^{-1}; bands specific for amide bonds occur in the range from 1550 to 1650 cm^{-1} and at 3300 cm^{-1}. Bands at 158 and 280 cm^{-1} (2a) and a broad band between 100 and 300 cm^{-1} (2b) are indicative for calcite lattice vibrations and ACC, respectively; CO_3 stretching vibrations (3a, b) at 1088 and 1083 cm^{-1} are characteristic for calcite or ACC. The band at at 960 cm^{-1} (4) indicates the presence of phosphate, and those for N–H-hydrogen bonds at 3450 cm^{-1} (5) the presence of chitin. (C) Raman peak intensity-distribution images of calcite and carbonate obtained between crossed (0/90) and parallel (0/0) polarization filters show characteristic changes within clearly defined regions of dex. The multi-colour images (CR) show the carbonate to calcite peak intensity ratios, and the graphs on the left show average Raman spectra of two regions marked with a blue and a yellow star. (D) Cluster analysis illustrate the distribution of regions with similar Raman spectra. E) Diagram showing the mean CR values of the 30 corresponding crystal units in D.

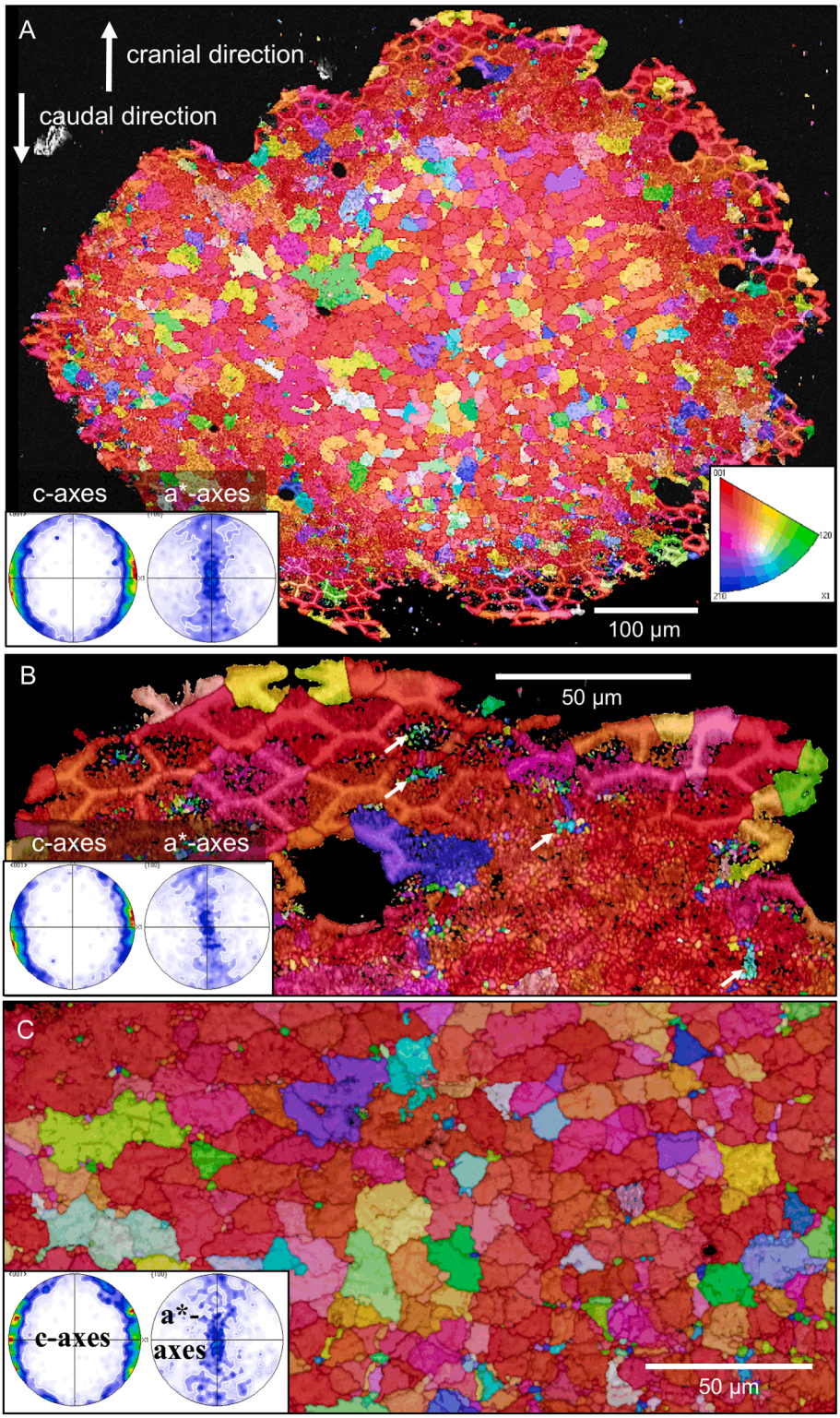

Fig. 10. Pattern of calcite orientation deduced from EBSD measurements on a tangential cut through the calcite layer of *Helleria brevicornis*. The cut surface is shown in Fig. S5. Crystal orientation is given color-coded, a similar color indicates similar crystallographic orientation of calcite crystalites. Pole figures given at each EBSD-map highlight the texture pattern. A) The calcite in *H. brevicornis* has a weak axial texture. The c-axes are within the plane of view. B) The pattern of calcite orientation in distal regions of the calcite layer. Well visible is a network of polygons outlined by peripheral calcite walls. The space within the walls of a polygon is filled with small, somewhat differently oriented, crystals. However, some crystals have a different orientation than the nearby polygon walls (white arrows). C) An EBSD map recorded on a cut within a proximal region of the calcite layer. These regions are formed of large calcite crystallites; the latter have irregular morphologies and interlink strongly. A polygonal pattern is present as well (see Fig. 11B) but less visible than in distal regions. The comparison of pole figures of Fig. 10B and C highlights that there is no difference between the texture of distal and proximal calcite layer sections.

wetting of the cuticle surface.

4.2. The exo- and endocuticle

The total thickness of the cuticle was only slightly higher in *H. brevicornis* (about 80–90 µm) than in *T. europaeus* (60–90 µm), although the body of *H. brevicornis* is almost twice as large, resulting in a higher flexibility of the tergites. The distal layer of calcite is stiffer and harder than the cuticle mineralised with ACC (Ernst et al., 2020a; Ernst et al., 2020b; Seidl et al., 2018). In addition to the mineral phase, the fibre orientation may affect the stiffness of the cuticle, as the elastic modulus of a single chitin nanofibril is 119 GPa along the axial direction and 28 Gpa in the transverse direction (Nikolov et al., 2011). However, such an effect can be neglected as long as the fibre orientation rotates in a twisted plywood-like manner. In *H. brevicornis* the thickness of calcite of about 25 µm is rather constant across the dorsal part of the tergites,

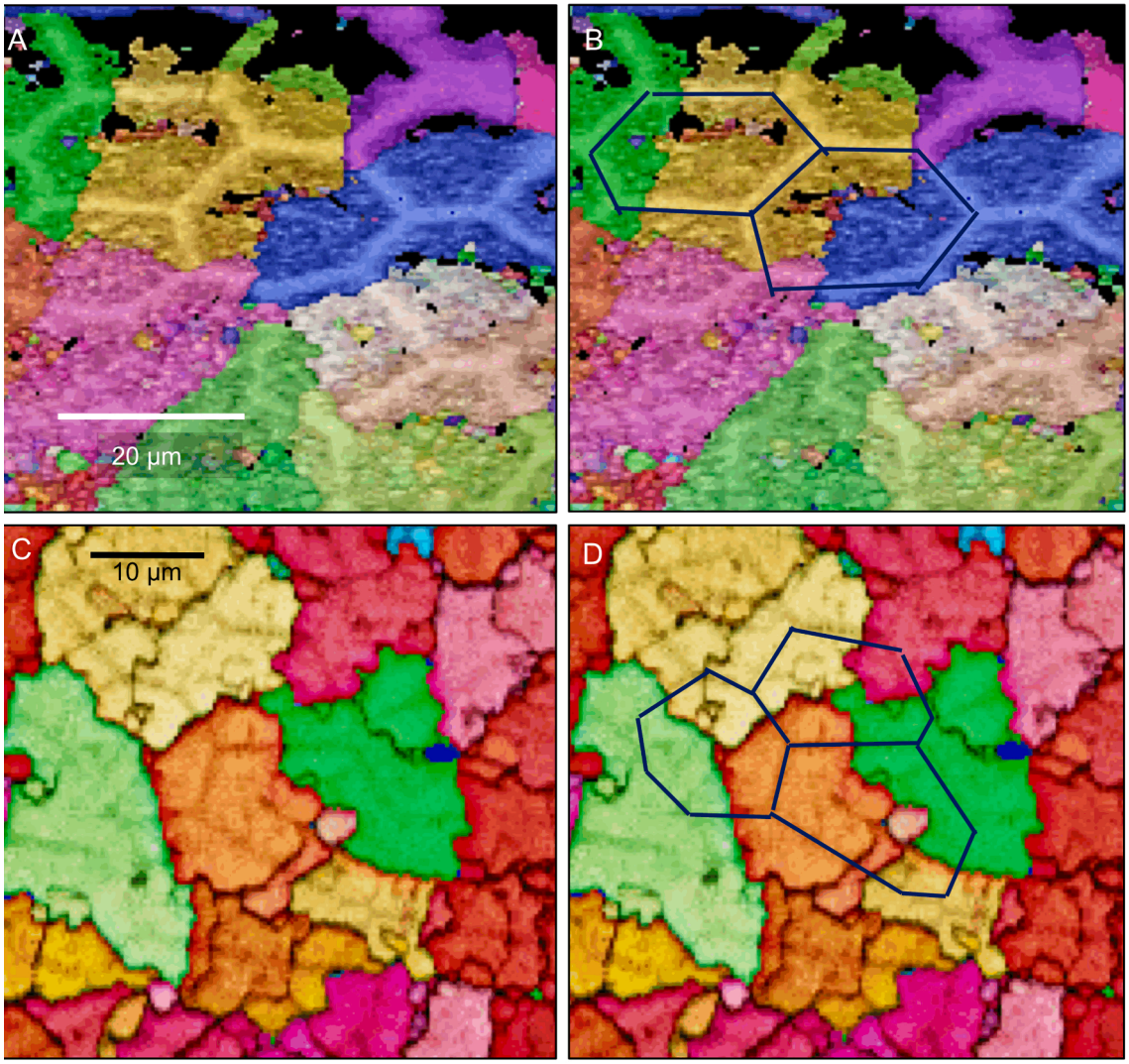

Fig. 11. Details of the EBSD maps shown in Fig. 13D and Fig. 10C depicting polygonal walls within distal domains of co-oriented crystals (A) and the calcite crystals in the proximal calcite layer (B). Note that most polygons contain calcite from more than one calcite unit.

while in *T. europaeus* it ranges between 10 µm between and up to 30 µm below the micro-tubercles. The thickness of the endocuticle as well as the abundance and structure of the pore canals is similar to that of *T. europaeus* (Seidl et al., 2011). However, the 50-nm thick, canal-like structures found in the proximal stacks of the endocuticle of *H. brevicornis* (Fig. 6D, E) have not yet been reported for any other isopod. The function of these structures remains unknown.

A differentiation of the exocuticle in a distal and a proximal layer as described here for *H. brevicornis* has so far been found in all detailed studies on the cuticle of terrestrial isopods (Fabritius et al., 2016). In terrestrial isopods other than Tylidae, the distal exocuticle is considerably thinner than the proximal exocuticle. In *Porcellio scaber* and *Armadilliudium vulgare* (both species belonging to the taxon Crinochaeta) for instance, the distal exocuticle is between 100 and 500 nm thick. Only below micro-tubercles it can have several µm (Ansenne et al., 1988; Seidl and Ziegler, 2012). The exocuticle of *H. brevicornis* very much resembles that of *T. europaeus* (Seidl et al., 2011). In contrast to the non-tylid species they have a very thick distal exocuticle and a thin proximal exocuticle that is separated from the distal layer by a thin middle layer. In both species, the organic matrix within the distal exocuticle consists of sparsely distributed organic fibres, formed by several chitin fibrils within a protein matrix. The fibres in the distal exocuticle, and the fibrils within the proximal exocuticular layers and the endocuticle of the two species are arranged in a planar twisted plywood (compare Fig. 4A with 14A). A distal-type exocuticle as found in Tylidae have also been reported as a "procuticule distale" in the marine isopod *Sphaeroma serratum* (Ansenne et al., 1988). However, in fractured *S. serratum* tergites the surface of the distal exocuticle has a rough appearance (Fig. 14B) in contrast to the smooth and polyhedral structures found in the Tylidae.

4.3. Distribution of the mineral phases

The cuticle of all marine and terrestrial isopods for which the mineral phase composition was studied contains calcite, ACC and little ACP (Alagboso et al., 2014; Becker et al., 2005; Ernst et al., 2020b; Hild et al., 2008; Hild et al., 2009; Neues et al., 2007; Ruangchai et al., 2013; Seidl et al., 2011). Crustaceans are the only major taxon where ACC is widely used for structural purposes (Addadi et al., 2003), presumably due to its high solubility (Brečević and Nielsen, 1989), which allows for rapid mobilisation of calcium and carbonate ions (Becker et al., 2005; Fabritius and Ziegler, 2003; Neues et al., 2011) and its mechanical isotropy (Weiner et al., 2003). The presence of stable ACC within the cuticle of isopods was first mentioned for *Oniscus asellus* comparing the exuviae with fresh cuticle using infrared spectroscopy (Wood and Russell, 1987). Fully electron amorphous calcium carbonate was demonstrated for the large sternal calcium carbonate deposits of *P. scaber*. For this purpose,

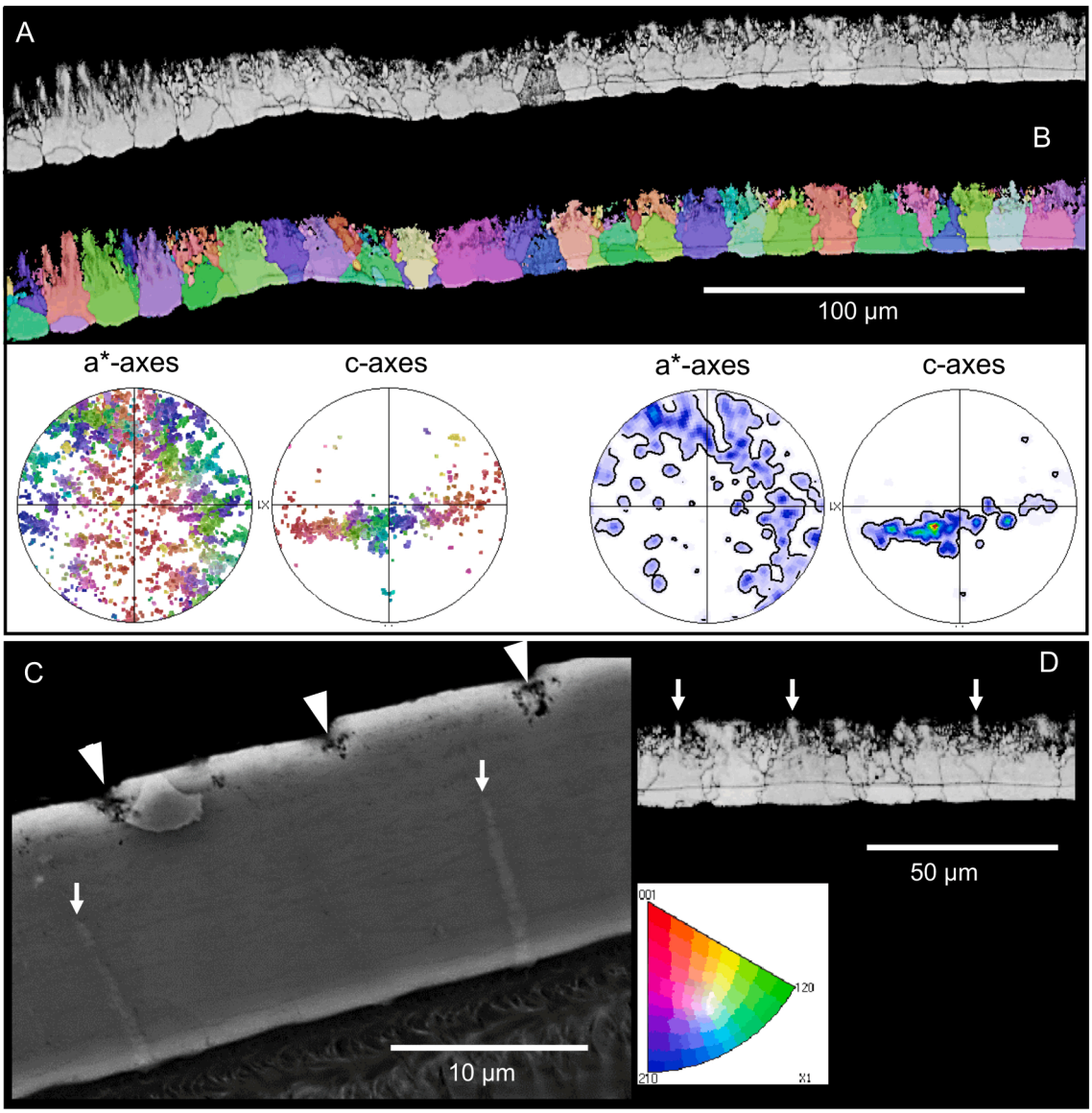

Fig. 12. Microstructure and texture of calcite deduced from EBSD measurements on a sagittal cut through the calcite layer of *Helleria brevicornis* (A, B, D). The grey-scaled image in A and D is a band contrast measurement image, also deduced from EBSD. The coloured image in (A) gives color-coded calcite orientation. C) BSE image taken on the sagittal cut through the calcite layer. A, B) The distal region of the calcite layer contains thin irregularly shaped extensions from large calcite units and small crystals with a different orientation than the subjacent large calcite units. Within the proximal region of the calcite layer the large crystals are interlinked to each other. B) The orientation pattern of the small crystals follows generally that of the mineral units comprising the proximal region of the calcite layer. C, D) White arrows point to vertical walls of calcite that are denser than the surrounding material in the proximal region of the calcite layer (C). The arrowheads point to regions devoid of mineral, that correspond to thick epicuticular material below scales (see Fig. 3C).

the diffraction patterns of the same area were compared before and after intensive irradiation with the electron beam leading to crystallisation of the ACC (Ziegler, 1994). Raman spectroscopy is the best and most useful method to distinguish between amorphous and crystalline calcium carbonate phases (Weiner et al., 2003). The spatial distribution of ACC and calcite in tergite cuticle of terrestrial isopods using SCμ-RSI was first reported by Hild et al. (2008). This study shows that in *P. scaber* and *A. vulgare,* the distal and proximal exocuticle is almost completely mineralized with calcite and the endocuticle only with ACC and little ACP. It appears that in terrestrial isopods living in extreme habitats the distribution of mineral phases may be different. In the cave dwelling isopod *Titanethes albus* (Trichoniscidae) the distal and part of the proximal exocuticle is mineralized with calcite (Hild et al., 2009), whereas in the large dessert isopod *Hemilepistus reaumuri* (Crinochaeta) distal parts of the endocuticle are also mineralised with calcite (Ernst et al., 2020b). The present study shows that in *H. brevicornis,* the thickness of the distal calcite layer shown by SCμ-RSI corresponds well with that of the distal exocuticle. The sharp and straight boundary between the distal calcite layer and the proximal layer of ACC corresponds with the proximal boundary of the distal exocuticle. The higher density of calcium within the distal exocuticle compared to the middle layer and the proximal exocuticle also indicates that calcite is confined to the distal exocuticle. Thus, the two more proximal layers of the exocuticle and the endocuticle are mineralized with ACC and ACP. Such a distribution of mineral phases has been found for *T. europaeus* as well (Seidl et al., 2011). The weight percentage of ACC of 59% within the tergite cuticle of *H. brevicornis* is higher than that of 48% in *T. europaeus* at the expense of lower concentrations of organic material and calcite (Seidl et al., 2011). The restriction of calcite to a very thick distal exocuticle and the presence of thin proximal exocuticular layers in both genera suggests that these features are a common characteristic of the Tylidae.

There is a difference in the calcite distribution between maps

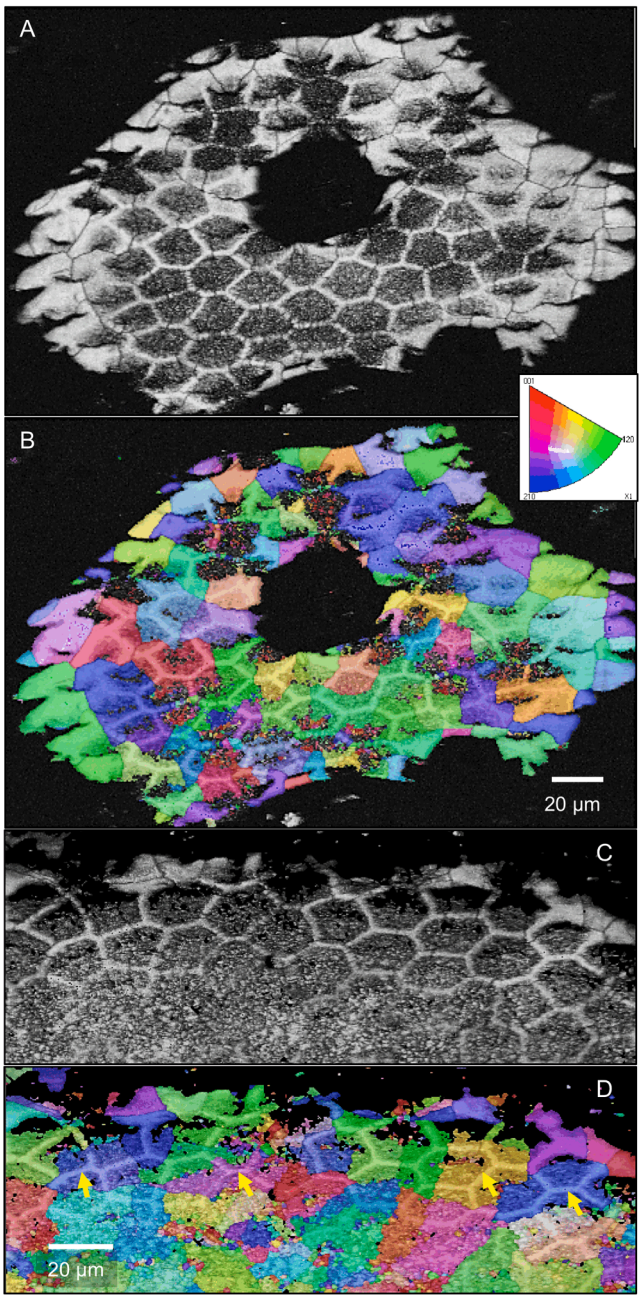

Fig. 13. EBSD measurements taken on tangential cuts through the uppermost region of the calcite layer. Fig. 12A, C are band contrast measurement images, Fig. 12B, D give calcite orientation color-coded. In both measurements (A, B) and (C, D) the network of polygons formed of calcite is well observable. B, D) It is further well observed that individual domains of co-oriented small crystals do not follow the polygonal pattern, but contain the calcite of the walls of polygons with similar orientation.

recorded with SCμ-RSI and EBSD. A sharp and straight boundary of calcite just below the epicuticle, as observed by SCμ-RSI and EPMA, is not recorded when the layer of calcite is imaged with EBSD (Fig. 11). This can occur when Kikuchi-patterns from the calcite cannot be indexed automatically by the EBSD software. The phenomenon was previously observed for the tergite cuticle of *H. reaumuri*, probably caused by the presence of very small calcite crystals or overlap of small crystals (Ernst et al., 2020b).

4.4. The magnesium and phosphate content

Magnesium and phosphate are known to favour the stabilization of ACC (Aizenberg et al., 2002; Bachra et al., 1963; Reddy, 1977). The magnesium content in the tergite cuticle of *H. brevicornis* is about half of that in *T. europaeus,* which is about one wt%. *T. europaeus* has the highest value measured in 10 different terrestrial isopod species (Ernst et al., 2020b). This can be explained by the ready access of the species to sea water, which contains 40 mmol L^{-1} magnesium. In most terrestrial isopods, the ratio of magnesium between the calcite crystal lattice and the non-calcite phases of the tergite cuticle is less than 0.2 (Neues et al., 2007). In *H. brevicornis* this value is greater with 0.5. However, this ratio is still much lower than in the tergite cuticle of *T. europaeus* (1.4) and *H. reaumuri* (2.5) where most of the magnesium is within the calcite crystal lattice (Ernst et al., 2020b; Seidl et al., 2011), making the calcite harder (Elstnerovà et al., 2010). Comparison of the tergite cuticle of 10 different isopod species suggests that the ACC/calcite ratio is independent from the amount of phosphate, magnesium or organic content of the cuticle (Ernst et al., 2020b). Hennig et al. (2012) has shown that physiologic concentrations of magnesium (12 mmol L^{-1}) have a high influence on the shape and surface structure of calcite precipitated in the presence of the protein bovine serum albumin, but no strong effect on the mineral phase. On the other hand, 0.01% of protein isolated from the sternal ACC deposits of *P. scaber* stabilizes ACC precipitated from a physiologic saline devoid of phosphate (Hennig et al., 2012). This suggests that the amorphous state in the crustacean cuticle is stabilized by low concentrations of specific proteins rather than magnesium or phosphate.

4.5. The significance of interprismatic septa in the crustacean cuticle

Vertically oriented column-like structures of calcite within the distal exocuticle, which occur in addition to the smooth and polygonal regions in *H. brevicornis,* were previously described for *T. europaeus* (Seidl et al., 2011). They were initially regarded as a possible candidate for mineral-filled canals because there was no other indication for the presence of pore canals. Pore canals are thought to play a role in the transport of ions for cuticle mineralisation (Giraud-Guille, 1984; Roer and Dillaman, 1984; Roer, 1980). They are formed by extensions of the hypodermal cells during secretion of the cuticle. They can be either filled with mineral or devoid of mineral, depending on differences in the sequence of mineral deposition and degeneration of the cell extensions (Compère and Goffinet, 1987). However, as the TEM and STEM micrographs show that pore canals end below the middle layer of the exocuticle (Fig. 5B, D), it becomes clear that in *H. brevicornis* the distal exocuticle has no pore canals. An alternative interpretation, based on the spatial distribution of the column-like structures in *H. brevicornis* is, that they correspond to interprismatic septa (Fabritius et al., 2016). Interprismatic septa are the initiation sites for calcification described for the cuticle of the Atlantic shore crab *Carcinus maenas* (Giraud-Guille, 1984). They are formed at the margins of the hypodermal cells resulting in a pattern of asymmetrical polygons imprinted in the organic matrix of the cuticle and containing the enzyme carbonic anhydrase (Giraud, 1981; Giraud-Guille, 1984). For the blue crab *Callinectes sapidus* it has been demonstrated that mineralisation does indeed commence at these septa (Dillaman et al., 2005). The polygonal pattern of mineral walls in the distal exocuticle of *H. brevicornis* observed in samples fractured horizontally and the organic material within the walls of the polygons, which differs from the chitin-protein fibres of the twisted plywood, support the interpretation that the mineral walls correspond to interprismatic septa. So far, these septa have only been reported from the exocuticle in crabs.

In the cuticle of *C. sapidus*, mineralisation occurs first at the distal side just underneath the epicuticle and at the distal and proximal side of the interprismatic septa. After the septa are fully mineralized in the vertical direction, mineralisation begins in the horizontal direction

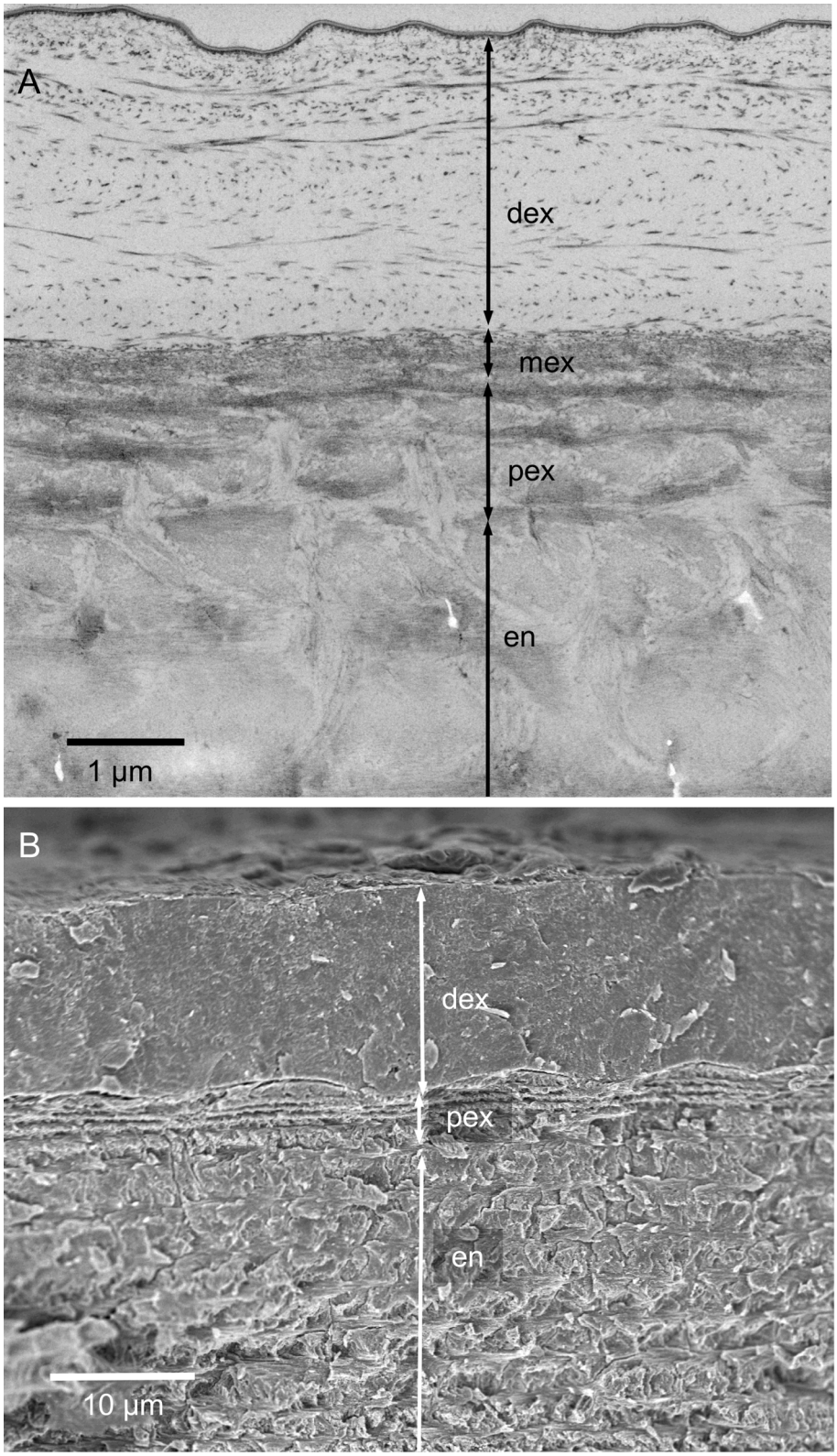

Fig. 14. A) STEM micrograph of the exo and endocuticle of the terrestrial isopod *Tylos europaeus*, depicting the similarity to the cuticle of *Helleria brevicornis* shown in Fig. 3A. B) Sagittally fractured sample of a non-demineralised tergite cuticle of the marine isopod *Sphaeroma serratum*. The surface of the distal exocuticle has a rough appearance in contrast to the smooth and polyhedral structures found in the Tylidae.

starting at the interprismatic septa from which it continues towards the centre of the polygonal spaces (Dillaman et al., 2005). The structure of fractured surfaces through the distal exocuticle suggest a similar horizontal growth pattern for *H. brevicornis*. The fan-shaped mineral structures extending horizontally from the margin of the interprismatic septa (Fig. 4C, D) suggest that mineral is first deposited at the organic material within the septa forming the mineral walls. Following the description of mineralisation in *C. sapidus* (Dillaman et al., 2005), we

propose that in a second step mineral would then form at deposition sites at the lateral margins of the septa, from which mineral would be deposited towards the centres of the polygonal spaces between the interprismatic septa. The fan-shaped horizontal appearance of mineral near the septa (Fig. 4C, D) is likely a result of competitive growth from neighbouring mineral nucleation sites at the interprismatic septa. When the mineral growth fronts emanating from the opposing polygonal septa meet in the centre of the prismatic space, they form the polygonal structure found in sagittally fractured surfaces in the distal exocuticle of *H. brevicornis* (Fig. 4A herein) and in *T. europaeus* (Fig. 4A in Seidl et al. (2011)). This polygonal appearance, which differs from the polygonal pattern formed by the interprismatic septa, is formed when the spread of the mineralisation is obstructed by the mineralisation fronts from the opposite sides, as sketched in Fig. 5C in Fabritius et al. (2016). Obviously, there is some fracture preference along the interface between these polygons (Fig. 4 A). The nano-sized granules observed on fractured surfaces of the distal exocuticle suggest that calcium carbonate is initially deposited as ACC before crystallising to calcite. This is in agreement with previous studies on mineral deposition in the tergite exocuticle of the terrestrial isopod *Porcellio scaber* (Neues et al., 2011), which showed by SCμ-RSI that within one hour after moulting calcium carbonate is deposited as ACC and then crystallises to calcite in situ within one day (Fig. 7A-C in Neues et al. (2011)). An ACC precursor phase for calcite has also been proposed for the dorsal branchial cuticle of *C. sapidus* (Dillaman et al., 2005), due to the high solubility of the mineral, which is deposited first on the interprismatic septa and then in the polygonal space between the septa.

4.6. The formation of co-oriented calcite units

It was surprising that interprismatic septa can be seen in the EBSD maps of *H. brevicornis*, in particular within distal regions of the distal exocuticle. In the distal region of the calcite layer this is due to a higher co-orientation of the calcite within the interprismatic septa compared to the calcite within the polygonal spaces.

The mean size of co-oriented calcite units within the distal exocuticle of *H. brevicornis* have roughly the size, but not the shape, of the polygons formed by the interprismatic septa that mark the boundaries of the hypodermal cells. The EBSD maps show that the interprismatic septa are situated within the calcite units and never around them. This shows, since the interprismatic septa mark the margins of the hypodermal cells (Giraud-Guille, 1984), that several hypodermal cells secrete the mineral for the formation of a single calcite-unit and each cell contribute to the formation of more than one. The high co-orientation of the mineral on either side of a septum separating two polygonal spaces suggests that the septa determine the orientation of calcite crystallites. From the observations acquired by FE-SEM of samples fractured in the native, non-demineralised state (Fig. 4C, D), the spatial relationship between calcite crystals and the interprismatic septa (Fig. 11) observed with EBSD, and the mineralisation sequence described for the blue crab exocuticle (Dillaman et al., 2005) we propose the following hypothetical model of calcite-unit formation in *H. brevicornis*: 1) In the initial state, the mineral consists of ACC within and between the interprismatic septa. 2) Calcite formation initially occurs through a phase transition from ACC within the interprismatic septa. 3) From both sides of crystallized septa, which delimit two adjacent polygonal spaces, crystallisation spreads towards the centres of the polygonal spaces. 4) During the transition of ACC to calcite within the polygonal space the growing crystal maintains about the orientation of the nearby interprismatic septa. 5) Crystallisation stops within a polygonal space when ACC is depleted from crystals forming from one or more septa surrounding the polygonal space. 6) Large crystals form when the calcite within the interprismatic septa of two or more neighbouring polygons have the same orientation. This hypothetical model can explain only the formation of large calcite units and not that of small calcite crystals that occur in the very distal region of the calcite layer and which have a different orientation than the nearby interprismatic septa (Fig. 13B). It is possible that this misorientation is related to the much denser distribution of chitin-protein fibres within the very distal region of the calcite layer (Fig. 3A), which may interfere with uniform crystallization of calcite from ACC.

The strong preference for the horizontal calcite c-axis orientation in the tergite cuticle of *H. brevicornis* with only some preference to the lateral sides of the animal is striking, especially as the c-axis orientation within the horizontal plane is almost at random. It indicates a well-tuned balance between anisotropic and isotropic mechanical properties of the tergite cuticle of *H. brevicornis*. Within terrestrial isopods there is high variation in the distribution of crystallographic orientation of calcite within the cuticle, which is related to the function of the cuticle and the habitat and behaviour of the animal (Ernst et al., 2020a; Ernst et al., 2020b; Huber et al., 2014; Huber et al., 2015; Seidl et al., 2012; Seidl et al., 2018). This relationship suggests that crystal orientation distribution is genetically controlled. The mechanism for this control, however, are completely unknown. Terrestrial isopods that can roll into a sphere rely entirely on their hard and stiff cuticle when not rolling out of sight for the predator (Schmalfuss, 1984). Due to the spherical shape, it is not possible to predict from which side a predator will attack, which makes an isotropic cuticle advantageous. A preferential orientation of the c-axis either parallel or perpendicular to the cuticle surface is advantageous when pore canals and especially the vertical fibrils therein are absent. Without vertically oriented fibrils, horizontal planes of parallel organic fibrils within the twisted plywood will easily delaminate if not stabilised by minerals. However, since calcite is brittle and easily cleaves along its cleavage planes, calcite should not be oriented in a way that the cleavage plane is parallel to the organic fibres. Delamination is prevented when many of the horizontal fibres run through the calcite cleavage planes. This is the case when the c-axis of calcite is oriented either vertically or horizontally (Fabritius et al., 2016). In tergites of *T. europaeus* such a strict horizontal c-axis orientation within the distal exocuticle has not been observed although pore canals are lacking as well. This difference between the two Tylid species may be explained by the higher mechanical stress the tergites of *H. brevicornis* have to sustain due to the higher flexibility of the larger tergites. In *T. europaeus* a strict horizontal c-axes orientation has been observed in the base region of the partes incisivae of the mandibles (Huber et al., 2015) but not in the tergites (Seidl et al., 2018). The largest muscles of isopods are found in the mandibles (Schmalfuss, 2008) suggesting that the cuticle of the partes incisivae are exposed to much higher mechanical loads than the tergites. This suggests that a strict c-axes orientation preference parallel to the surface is required only when the cuticle has to sustain very high mechanical loads.

5. Summary and conclusions

H. brevicornis is the only member of the Tylidae that does not live along seashores, but occurs in forests at altitudes of up to 1200 m. Like its relatives, it can roll up into a sphere when disturbed and burrows into the substrate. The comparison with the beach isopod *T. europaeus* revealed that there are common and different structural features of the tergite cuticle. The differences mainly concern the epicuticle and surface structures, such as the absence of micro-tubercles in *H. brevicornis* and the presence of two types of tricorn sensilla with brushed tips and the higher number of wax layers within the epicuticle. The ultrastructure of the exo- and endocuticle of *H. brevicornis* and *T. europaeus* are very similar. Although *H. brevicornis* is much larger than *T. europaeus,* the overall thickness of the tergite cuticle are as well similar. In both species calcite is restricted to the distal exocuticle, which appears to be a characteristic feature of Tylidae. It is characterised by sparsely distributed organic fibres consisting of several chitin fibrils within a protein matrix, arranged in a planar twisted plywood. Most striking is the presence of interprismatic septa within the distal exocuticle, which serve as initiation sites for mineralisation and have previously only been

reported from decapod crabs. As has been shown for a number of Crustacea, including isopods, mineralisation with calcium carbonate initially occurs in the form of ACC. The present study suggests that calcite formation also begins in the interprismatic septa and that calcite formation spreads from these to the centres of adjacent polygonal prisms bounded by the septa. Furthermore, the results suggest that crystallisation initiation sites in and at the septa help to control the size, shape and distribution of the co-oriented calcite units.

CRediT authorship contribution statement

Bastian Seidl: Methodology, Investigation, Visualization, Writing - original draft. **Christian Reisecker:** Investigation. **Frank Neues:** Investigation. **Alessandro Campanaro:** Resources. **Matthias Epple:** Methodology, Supervision. **Sabine Hild:** Methodology, Supervision. **Andreas Ziegler:** Conceptualization, Methodology, Investigation, Visualization, Writing - original draft, Visualization, Supervision, Funding acquisition.

Declaration of Competing Interest

The authors declare that they have no known competing financial interests or personal relationships that could have appeared to influence the work reported in this paper.

Acknowledgement

We thank Dr. Erika Griesshaber Department of Earth and Environmental Sciences and GeoBioCenter at the LMU Munich for the kind supply of the EBSD, BSE and band contrast images. This work was supported by the the Deutsche Forschungsgemeinschaft (DFG) within the priority programs SPP 1420 [Zi 368/8-1].

Appendix A. Supplementary data

Supplementary data to this article can be found online at https://doi.org/10.1016/j.yjsbx.2021.100051.

References

Addadi, L., Raz, S., Weiner, S., 2003. Taking advantage of disorder: amorphous calcium carbonate and its roles in biomineralization. Adv. Mater. 15 (12), 959–970.
Aizenberg, J., Lambert, G., Weiner, S., Addadi, L., 2002. Factors involved in the formation of amorphous and crystalline calcium carbonate: a study of an ascidian skeleton. J. Am. Chem. Soc. 124, 32–39.
Alagboso, F.I., Reisecker, C., Hild, S., Ziegler, A., 2014. Ultrastructure and mineral composition of the cornea cuticle in the compound eyes of a supralittoral and a marine isopod. J. Struct. Biol. 187 (2), 158–173.
Altner, H., Prillinger, L., 1980. Ultrastructure of invertebrate chemo-, thermo- and hygroreceptors and its functional significance. Int. Rev. Cytol. 6, 69–139.
Ansenne, A., Compère, P., Goffinet, G., 1988. Organisation, sclérotisation et composition minérale des sclérites d'une espèce d'isopode marin et de quatre espèces d'isopodes terrestres oniscoïdes. Actes de Colloques 8, 39–46.
Bachra, B.N., Trautz, O.R., Simon, S.L., 1963. Precipitation of calcium carbonates and phosphates. I. Spontaneous precipitation of calcium carbonates and phosphates under physiological conditions. Arch. Biochem. Biophys. 103 (1), 124–138.
Becker, A., Ziegler, A., Epple, M., 2005. The mineral phase in the cuticles of two species of Crustacea consists of magnesium calcite, amorphous calcium carbonate, and amorphous calcium phosphate. Dalton Trans. 2005, 1814–1820.
Becker, A., Bismayer, U., Epple, M., Fabritius, H., Hasse, B., Shi, J., Ziegler, A., 2003. Structural characterisation of X-ray amorphous calcium carbonate (ACC) in sternal deposits of the Crustacea *Porcellio scaber*. Dalton Trans. 2003, 551–555.
Blackwell, J., Weih, M.A., 1980. Structure of chitin-protein complexes: ovipositor of the ichneumon fly *Megarhyssa*. J. Mol. Biol. 137 (1), 49–60.
Bouligand, Y., 1972. Twisted fibrous arrangements in biological materials and cholesteric mesophases. Tissue Cell 4 (2), 189–217.
Brečević, L., Nielsen, A.E., 1989. Solubility of amorphous calcium carbonate. J. Crystal Growth 98 (3), 504–510.
Carlström, D., 1957. The crystal structure of α-chitin. J. Biophysic. Biochem. Cytol. 3, 669–683.
Collinge, W.E., 1941. XL.- Some remarks on the Genus Helleria von Ebner (Terrestrial Isopoda). Ann. Mag. Nat. Hist. 8, 522–526.
Compère, P., 1990. Fine structure and elaboration of the epicuticle and the pore canal system in tergite cuticle of the land isopod *Oniscus asellus* during a moulting cycle. In: Juchault, P., Mocquard, J.P. (Eds.), The Biology of Terrestrial Isopods III. Université de Portiers, pp. 169–175.
Compère, P.h., Goffinet, G., 1987. Elaboration and ultrastructural changes in the pore canal system of the mineralized cuticle of *Carcinus maenas* during the moulting cycle. Tissue & Cell 19 (6), 859–875.
Dillaman, R., Hequembourg, S., Gay, M., 2005. Early pattern of calcification in the dorsal carapace of the Blue Crab, *Callinectes sapidus*. J. Morphol. 263 (3), 356–374.
Dimitriou, A.C., Taiti, S., Sfenthourakis, S., 2019. Genetic evidence against monophyly of Oniscidea implies a need to revise scenarios for the origin of terrestrial isopods. Sci. Rep. 9, 18508.
Edney, E.B., 1968. Transition from water to land in isopod crustaceans. Am. Zool. 8 (3), 309–326.
Elstnerovà, P., Friák, M., Fabritius, H.O., Lymperakis, L., Hickel, T., Petrov, M., Nikolov, S., Raabe, D., Ziegler, A., Hild, S., Neugebauer, J., 2010. Ab initio study of thermodynamic, structural, and elastic properties of Mg-substituted crystalline calcite. Acta. Biomater. 6, 4506–4512.
Erhard, F., 1997. Das pleonale Skelet-Muskel-System von *Titanethes albus* (Synocheta) und weiterer Taxa der Oniscidea (Isopoda), mit Schlußfolgerungen zur Phylogenie der Landasseln. Stuttg. Beitr. Naturk. 550, 1–70.
Ernst, F., Fabritius, H., Griesshaber, E., Schmahl, W.W., Ziegler, A., 2020a. The edge regions in tergites of the desert isopod Hemilepistus reaumuri: the transition from hard cuticle to flexible arthrodial membrane. Appl. Phys. A 126, Article number: 793.
Ernst, F., Fabritius, H.-O., Griesshaber, E., Reisecker, C., Neues, F., Epple, M., Schmahl, W.W., Hild, S., Ziegler, A., 2020b. Functional adaptations in the tergite cuticle of the desert isopod *Hemilepistus reaumuri* (Milne-Edwards, 1840). J. Struct. Biol. 212 (1), 107570. https://doi.org/10.1016/j.jsb:2020.107570.
Fabritius, H., Ziegler, A., 2003. Analysis of Ca CO_3 deposit formation and degradation during the molt cycle of the terrestrial isopod *Porcellio scaber* (Crustacea, Isopoda). J. Struct. Biol. 142 (2), 281–291.
Fabritius, H., Walther, P., Ziegler, A., 2005. Architecture of the organic matrix in the sternal $CaCO_3$ deposits of *Porcellio scaber* (Crustacea, Isopoda). J. Struct. Biol. 150 (2), 190–199.
Fabritius, H.-O., Ziegler, A., Friák, M., Nikolov, S., Huber, J., Seidl, B.H.M., Ruangchai, S., Alagboso, F.I., Karsten, S., Lu, J., Janus, A.M., Petrov, M., Zhu, L.-F., Hemzalová, P., Hild, S., Raabe, D., Neugebauer, J., 2016. Functional adaptation of crustacean exoskeletal elements through structural and compositional diversity: a combined experimental and theoretical study. Bioinspir. Biomim. 11.
Gentile, G., Campanaro, A., Carosi, M., Sbordoni, V., Argano, R., 2010. Phylogeography of *Helleria brevicornis* Ebner 1868 (Crustacea, Oniscidea): Old and recent differentiations of an ancient lineage. Mol. Phylogenet. Evol. 54 (2), 640–646.
Giraud, M.M., 1981. Carbonic anhydrase activity in the integument of the crab Carcinus maenas during the internolt cycle. Comp. Biochem. Physiol. 69, 381–387.
Giraud-Guille, M.-M., 1984. Calcification initiation sites in the crab cuticle: the interprismatic septa. Cell Tissue Res. 236, 413–420.
Goldsmith, J.R., Graf, D.L., 1958. Relation between lattice constants and composition of the Ca-Mg carbonates. Am. Mineral. 43, 84–101.
Grunenfelder, L.K., Herrera, S., Kisailus, D., 2014. Crustacean-derived biomimetic components and nanostructured composites. Small 10 (16), 3207–3232.
Hadley, N.F., Warburg, M.R., 1986. Water loss in three species of xeric-adapted isopods: correlations with cuticular lipids. Comp. Biochem. Physiol. 85 (4), 669–672.
Hatanaka, T., 1989. Responses of dorsal tricorn-type sensilla on *Ligia exotica*. Comp. Biochem. Physiol. 92 (4), 513–519.
Hennig, S., Hild, S., Fabritius, H.-O., Soor, C., Ziegler, A., 2012. Influence of near-physiological salines and organic matrix proteins from amorphous $CaCO_3$ deposits of *Porcellio scaber* on in vitro $CaCO_3$ precipitation. Cryst. Growth Design 12 (2), 646–655.
Hild, S., Marti, O., Ziegler, A., 2008. Spatial distribution of calcite and amorphous calcium carbonate in the cuticle of the terrestrial crustaceans *Porcellio scaber* and *Armadillidium vulgare*. J. Struct. Biol. 163 (1), 100–108.
Hild, S., Neues, F., Žnidaršič, N., Štrus, J., Epple, M., Marti, O., Ziegler, A., 2009. Ultrastructure and mineral distribution in the tergal cuticle of the terrestrial isopod *Titanethes albus*. Adaptations to a karst cave biotope. J. Struct. Biol. 168 (3), 426–436.
Holdich, D.M., 1984. The cuticular surface of woodlice: a search for receptors. Symp. Zool. Soc. Lond. 53, 9–48.
Holdich, D.M., Lincoln, R.J., 1974. An investigation of the surface of the cuticle and associated sensory structures of the terrestrial isopod, *Porcellio scaber*. J. Zool. London. 172, 469–482.
Huber, J., Fabritius, H.-O., Griesshaber, E., Ziegler, A., 2014. Function-related adaptations of ultrastructure, mineral phase distribution and mechanical properties in the incisive cuticle of mandibles of *Porcellio scaber* Latreille, 1804. J. Struc. Biol. 188 (1), 1–15.
Huber, J., Griesshaber, E., Nindiyasari, F., Schmahl, W.W., Ziegler, A., 2015. Functionalization of biomineral reinforcement in crustacean cuticle: calcite orientation in the partes incisivae of the mandibles of *Porcellio scaber* and the supralittoral species *Tylos europaeus* (Oniscidea, Isopoda). J. Struct. Biol. 190 (2), 173–191.
Knapp, M., Baehtz, C., Ehrenberg, H., Fuess, H., 2004a. The synchrotron powder diffractometer at beamline B2 at HASYLAB/DESY: status and capabilities. J. Synchorotron Rad. 11 (4), 328–334.
Knapp, M., Joco, V., Baehtz, C., Brecht, H.H., Berghaeuser, A., Ehrenberg, H., von Seggern, H., Fuess, H., 2004b. Position-sensitive detector system OBI for high resolution X-ray powder diffraction using on-site readable image plates. Nucl. Instr. Methods Phys. Res. A 521 (2-3), 565–570.

Michel-Salzat, A., Bouchon, D., 2000. Phylogenetic analysis of mitochondrial LSU rRNA in oniscids. C.R. Acad. Sci. Paris, Sciences de la vie/Life sciences 323, 827-837.
Neues, F., Ziegler, A., Epple, M., 2007. The composition of the mineralized cuticle in marine and terrestrial isopods: A comparative study. Cryst. Eng. Comm. 9 (12), 1245. https://doi.org/10.1039/b710789g.
Neues, F., Hild, S., Epple, M., Marti, O., Ziegler, A., 2011. Amorphous and crystalline calcium carbonate distribution in the tergite cuticle of moulting *Porcellio scaber* (Isopoda, Crustacea). J. Struct. Biol. 175 (1), 10–20.
Neville, A.C., Parry, D.A.D., Woodhead-Galloway, J., 1976. The chitin crystallite in arthorod cuticle. J. Cell. Sci. 21, 73–82.
Nikolov, S., Petrov, M., Lymperakis, L., Friák, M., Sachs, C., Fabritius, H.-O., Raabe, D., Neugebauer, J., 2010. Revealing the design principles of high-performance biological composites using ab initio and multiscale simulations: the example of lobster cuticle. Adv. Mat. 22 (4), 519–526.
Nikolov, S., Fabritius, H., Petrov, M., Friák, M., Lymperakis, L., Sachs, C., Raabe, D., Neugebauer, J., 2011. Robustness and optimal use of design principles of arthropod exoskeletons studied by ab initio-based multiscale simulations. J. Mech. Behav. Biomed. Mater. 4 (2), 129–145.
Powell, C.V.L., Halcrow, K., 1982. The surface microstructure of marine and terrestrial isopoda (Crustacea, Peracarida). Zoomorph. 101 (3), 151–164.
Price, J.B., Holdich, D.M., 1980. The formation of the epicuticle and associated structures in *Oniscus asellus* (Crustacea, Isopoda). Zoomorph. 94 (3), 321–332.
Reddy, M.M., 1977. Crystallization of calcium carbonate in the presence of trace concentrations of phosphorus-containing anions. J. Cryst. Growth. 41 (2), 287–295.
Rodriguez-Carvajal, J., 1990. FULLPROF: A program for rietveld refinement and pattern matching analysis., p. 127, Abstracts of the Satellite Meeting on Powder Diffraction of the XV Congress of the IUCr, Toulouse.
Roer, R., Dillaman, R., 1984. The structure and calcification of the crustacean cuticle. Am. Zool. 24 (4), 893–909.
Roer, R.D., 1980. Mechanisms of resorption and deposition of calcium in the carapace of the crab *Carcinus maenas*. J. Exp. Biol. 88, 205–218.
Ruangchai, S., Reisecker, C., Hild, S., Ziegler, A., 2013. The architecture of the joint head cuticle and its transition to the arthrodial membrane in the terrestrial crustacean *Porcellio scaber*. J. Struct. Biol. 182 (1), 22–35.
Schmalfuss, H., 1978. Morphology and function of cuticular micro-scales and corresponding structures in terrestrial isopod (Crust., Isop., Oniscoidea). Zoomorphology 91, 263–274.
Schmalfuss, H., 1984. Eco-morphological strategies in terrestrial isopods. Symp. Zool. Soc. Lond. 53, 49–63.
Schmalfuss, H., 2008. The mandibles in terrestrial isopods (Isopoda: Oniscidea). , p. 69–74, in: M. Zimmer, et al., (Eds.), Proceedings of the International Symposium of Terrestrial Isopod Biology-ISTIB-7, Shaker Verlag, Aachen.
Schmalfuss, H., Ferrara, F., 1978. Terrestrial isopods from West Africa. Monit. Zool. Ital. Supplemento 11 (1), 15–97.
Schmidt, U., Hild, S., Ibach, W., Hollricher, O., 2005. Characterization of thin polymer films on the nanometer scale with confocal raman AFM. Macromol. Symp. 230 (1), 133–143.
Seidl, B., Huemer, K., Neues, F., Hild, S., Epple, M., Ziegler, A., 2011. Ultrastructure and mineral distribution in the tergite cuticle of the beach isopod *Tylos europaeus* Arcangeli, 1938. J. Struct. Biol. 174 (3), 512–526.
Seidl, B.H.M., Ziegler, A., 2012. Electron microscopic and preparative methods for the analysis of isopod cuticle. ZooKeys 176, 73–85.
Seidl, B.H.M., Reisecker, C., Hild, S., Griesshaber, E., Ziegler, A., 2012. Calcite distribution and orientation in the tergite exocuticle of the isopods *Porcellio scaber* and *Armadillidium vulgare* (Oniscidea, Crustacea) - a combined FE-SEM, polarized SCμ-RSI and EBSD study. Z. Kristallogr. 227, 777–792.
Seidl, B.H.M., Griesshaber, E., Fabritius, H.-O., Reisecker, C., Hild, S., Taiti, S., Schmahl, W.W., Ziegler, A., 2018. Tailored disorder in calcite organization in tergite cuticle of the supralittoral isopod *Tylos europaeus* arcangeli, 1938. J. Struct. Biol. 204 (3), 464–480.
Vandel, A., 1960. Faune de France - Isopodes terrestres P. Lechevalier, Paris.
Vittori, M., Štrus, J., 2014. The integument in troglobitic and epigean woodlice (Isopoda: Oniscidea): a comparative ultrastructural study. Zoomorph. 133 (4), 391–403.
Weiner, S., Levi-Kalisman, Y., Raz, S., Addadi, L., 2003. Biologically formed amorphous calcium carbonate. Connect. Tissue. Res. 44 (1), 214–218.
Wood, C.T., Kostanjšek, R., Araujo, P.B., Štrus, J., 2017. Morphology, microhabitat selection and life-history traits of two sympatric woodlice (Crustacea: Isopoda: Oniscidea): a comparative analysis. Zool. Anz. 268, 1–10.
Wood, S., Russell, J.D., 1987. On the nature of the calcium carbonate in the exoskeleton of the woodlouse *Oniscus asellus* L. (Isopoda, Oniscoidea). Crustaceana 53 (1), 49–53.
Zaluzec, N.J., 1980. Thin film characterization using analytical electron microscopy. Thin Solid Films 72 (1), 177–192.
Ziegler, A., 1994. Ultrastructure and electron spectroscopic diffraction analysis of the sternal calcium deposits of *Porcellio scaber* Latr. (Isopoda, Crustacea). J. Struct. Biol. 112 (2), 110–116.
Ziegler, A., 2003. Variations of calcium deposition in terrestrial isopods, p. 299-309, in: S. Sfenthourakis, et al., (Eds.), The Biology of Terrestrial Isopods, V. Proceedings of the 5th International Symposium on the Biology of Terrestrial Isopods, Koninklijke Brill NV, Leiden.
Ziegler, A., Altner, H., 1995. Are the most numerous sensilla of terrestrial isopods hygroreceptors? Ultrastructure of the dorsal tricorn sensilla of *Porcellio scaber*. Cell Tissue Res. 282 (1), 135–145.